Energy Research and Development Division

FINAL PROJECT REPORT

Solar-Reflective "Cool" Walls: Benefits, Technologies, and Implementation

Appendix O: Development of Retroreflective Materials (Task 5.3 Report)

California Energy Commission
Gavin Newsom, Governor

April 2019 | CEC-500-2019-040-APO

Appendix O: Development of retroreflective materials (Task 5.3 report)

Ronnen Levinson[1], Sharon Chen[1], Jonathan Slack[1], Howdy Goudey[1], and Paul Berdahl[1]

[1] Heat Island Group, Lawrence Berkeley National Laboratory

29 June 2018

Abstract

Raising a city's albedo increases the fraction of incident sunlight returned to outer space, cooling cities and their buildings. Retroreflective cool walls could improve upon diffusely reflecting cool walls by reflecting incoming beam radiation to the solar disc (if the retroreflection is three dimensional and ideal) or at least upwards (if the retroreflection is two dimensional and/or imperfect). The greatest challenge in retroreflective wall design appears to be the need to operate at large incidence angles to reflect a substantial portion of incident sunlight. First-principle physics, ray tracing simulations, and solar spectral bi-directional reflectance intensity measurements suggest that it will be difficult to achieve this with surfaces that rely on total internal reflection.

Attempts to produce a two-surface retroreflector with orthogonal mirror grooves by cutting and polishing an aluminum block indicate that residual surface roughness impedes retroreflection. Ongoing efforts focus on shaping aluminized Mylar film, a material with very high specular reflectance across the solar spectrum.

1 Introduction

Raising a city's albedo increases the fraction of incident sunlight returned to outer space, cooling cities and their buildings. "Cool" horizontal surfaces with high solar reflectance, such as white roofs and light-colored pavements, are ideal solutions for a low-density city with short buildings, in which most of the sunlight is intercepted by roofs and pavements. However, in a densely populated urban area with many tall buildings, more sunlight falls on walls than on roofs or pavements. A large fraction of light that is diffusely reflected from a vertical surface can strike neighboring buildings, pavements, or pedestrians.

Figure 1 illustrates three idealized reflections: specular (perfectly mirrorlike), Lambertian (perfectly diffuse), and retro (back to source). We can increase the effective albedo of urban areas, and prevent heating of neighboring buildings, by making building walls retroreflective. A retroreflector, such as a cube-corner (Figure 2a), orthogonal groove (Figure 2b), or cat's eye (Figure 3) can return light toward its source. Retroreflective cool walls could improve upon diffusely reflecting cool walls by reflecting incoming beam radiation to the solar disc (if the retroreflection is three dimensional and ideal) or at least upwards (if the retroreflection is two dimensional and/or imperfect). This can increase the fraction of sunlight reflected out of the urban canyon formed by the walls of neighboring buildings and the ground between them.

Today, corner-cube and cat's eye retroreflectors are widely used for traffic safety, remote sensing, and optical communication. Here we consider the application of retroreflectors to exterior walls.

For example, consider an isolated building with 0.60 wall albedo and 0.20 ground albedo, each surface a Lambertian reflector. About 36% of the sunlight incident on the wall would return to the sky [0.60 wall albedo × (0.5 sky view factor + 0.5 ground view factor × 0.20 ground albedo)] (Figure 4a). If the wall were instead covered with a retroreflector of equal albedo—say, orthogonal mirror pairs, each surface of albedo 0.775, with a two-bounce albedo of 0.775^2 = 0.60 (Figure 2b)—it would reflect upward 60% of incident beam sunlight, and about 30% of the incident diffuse sunlight (of the 60% of diffuse light that is reflected, half will go up, and half will go down). If 20% of the incident sunlight is diffuse, the final fraction returned to the sky would be 80% × 0.60 wall solar retroreflectance + 20% × [0.60 wall solar diffuse reflectance × (0.5 sky view factor + 0.5 ground view factor × 0.20 ground albedo)] = 55% (Figure 4b).

A Lambertian wall would have to reflect 92% of incident sunlight to return 55% of incident sunlight to the sky [0.92 wall albedo × (0.5 sky view factor + 0.5 ground view factor × 0.20 ground albedo)] (Figure 4c).

Introducing a neighboring building reduces wall and ground sky view factors, but does not impede retroreflection. Hence the boost in skyward reflection offered by substituting a retroreflective wall for a Lambertian wall will be even greater for a wall within the urban canyon.

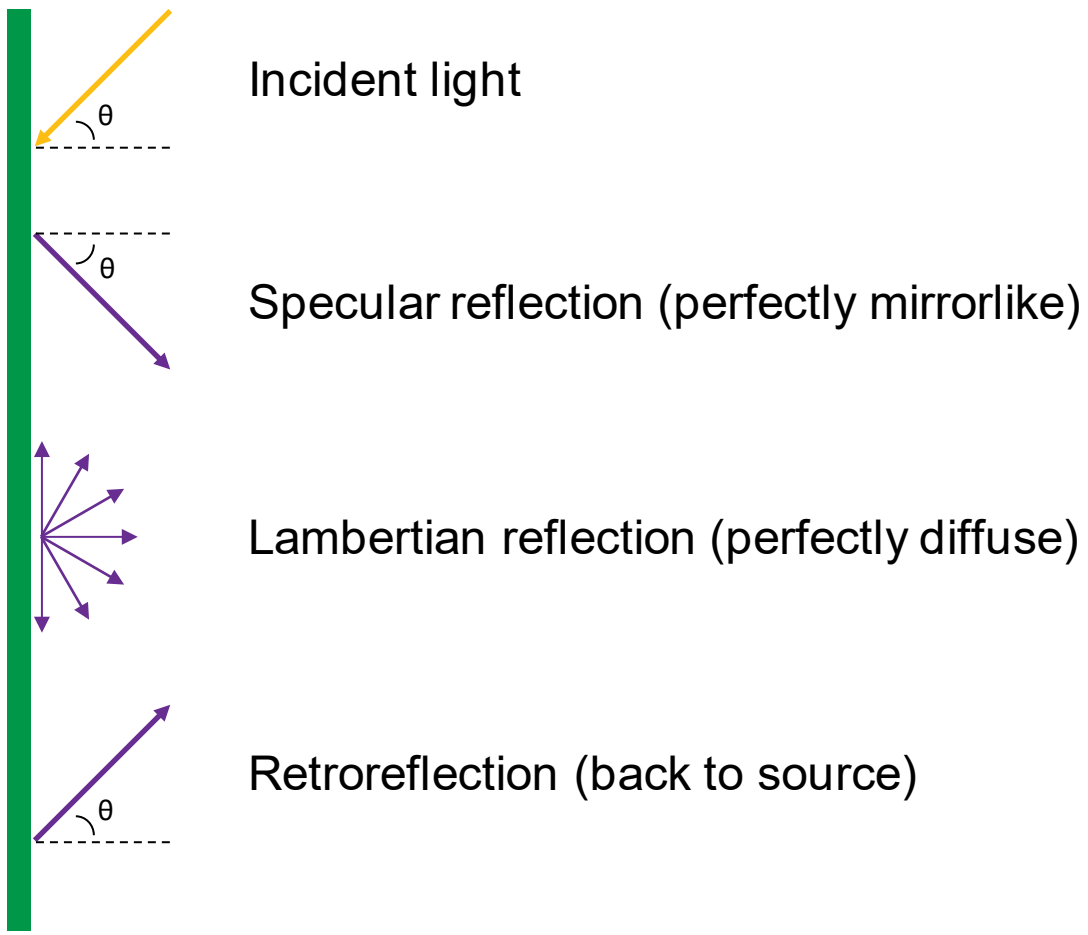

Figure 1. Specular, Lambertian, and retro reflection of beam light striking a vertical surface.

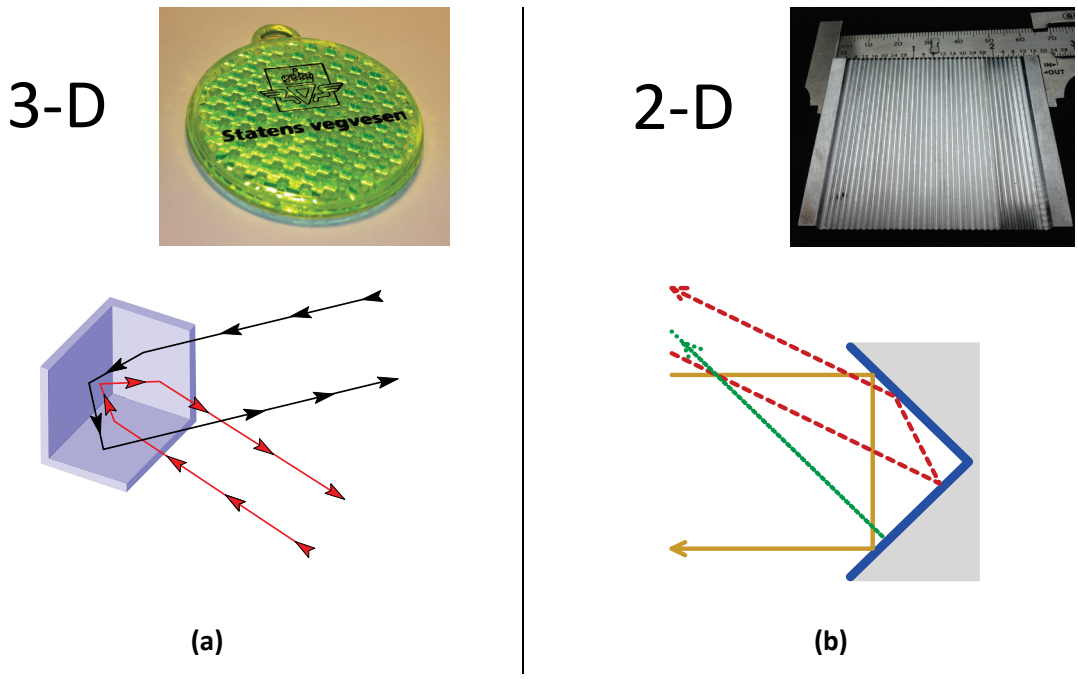

Figure 2. A retroreflector uses up to three orthogonal mirrors to return light to its source. Panel (a) shows a bicycle reflector comprised of three-mirror "cube corners" that will perfectly retroreflect any beam, while panel (b) shows a groove aluminum block comprised of two-mirror orthogonal groove that, if oriented with the block vertical and the grooves horizontal, will retroreflect about the horizontal plane and specularly reflect about the vertical plane.

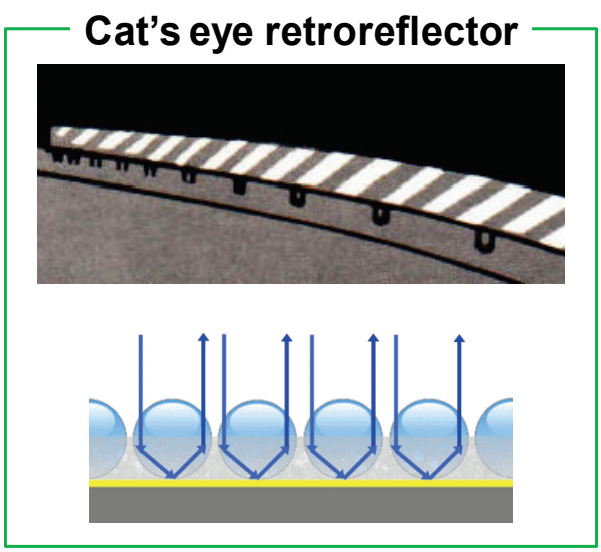

Figure 3. A cat's eye retroreflector, such as this safety paint, uses spheres of high real refractive index in a lower-index binder to provide three reflections that return light to its source.

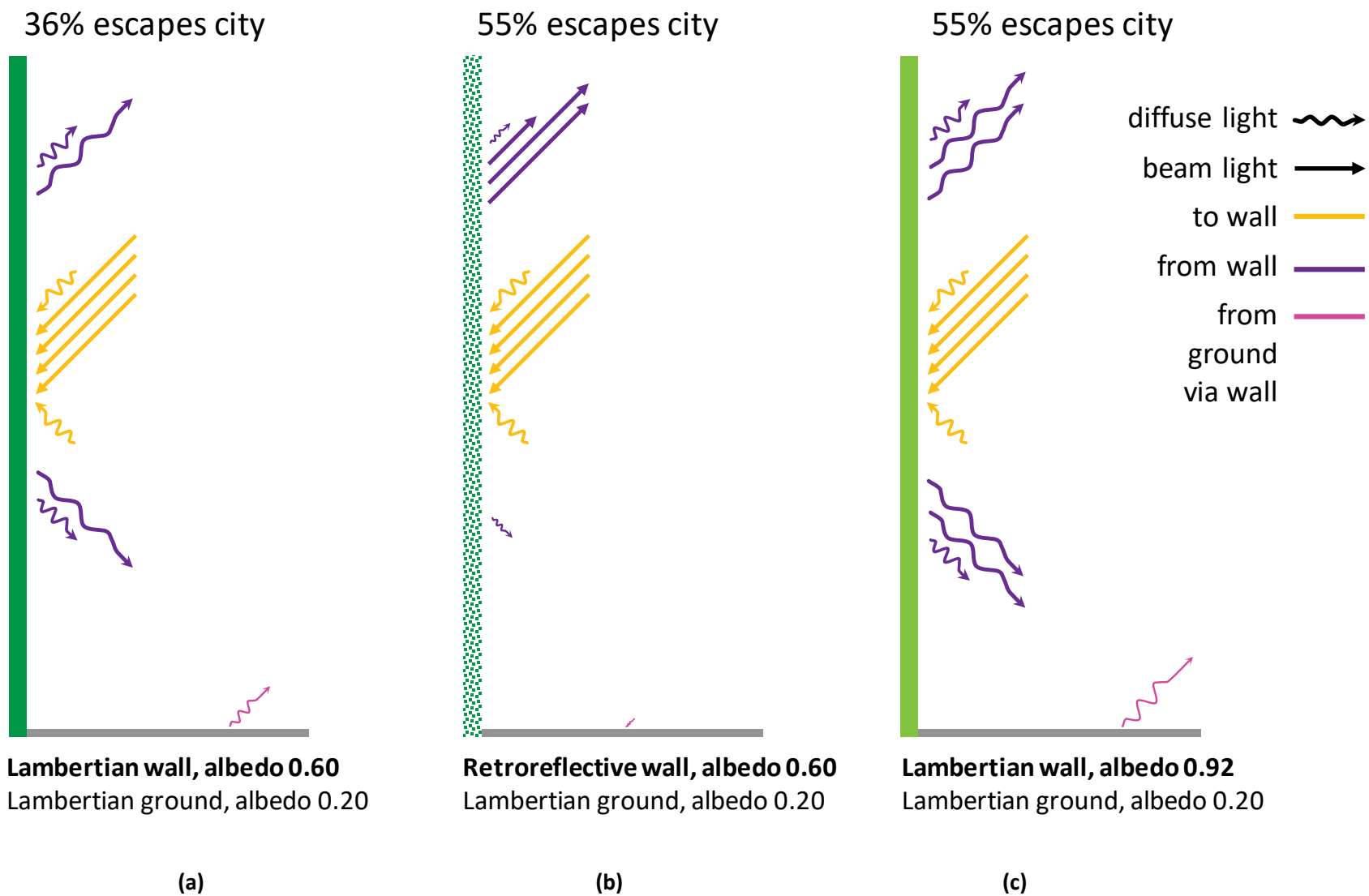

Figure 4. Retroreflective cool surfaces can help sunlight that strikes walls escape the city.

2 Design considerations

A safety retroreflector makes a sign easier to read in low light (e.g., at night, or in a tunnel) by reflecting vehicle headlamp illumination to the driver. If the sign is far away, making the path from sign to driver nearly parallel to that from headlamp to sign, modest retroreflection of headlamp light arriving at near-normal incidence will suffice. Only visible light (0.4 – 0.7 µm) need be reflected (ASTM 2017).

To reduce the solar heat gain of the building and its surroundings, a *wall* retroreflector must reflect a large fraction of incident sunlight. Sunlight will strike the wall over a wide range of incidence angles, and about half the radiative energy in sunlight arrives in the invisible near-infrared spectrum (0.7 – 2.5 µm) (Levinson et al. 2010). Thus, the design requirements for a wall retroreflector differ significantly from those for a safety retroreflector (Figure 5).

2.1 Solar spectral reflectance of mirrorlike surfaces

In principle, a transparent surface exhibiting total internal reflection (TIR) or a metal mirror can provide strong specular reflection over most or all of the solar spectrum (0.3 – 2.5 µm). Examples:

- Crown glass (e.g., Schott N-BK7) has a narrow range of real refractive index (n=1.48 – 1.56) over the entire solar spectrum. Its internal transmittance is greater than 0.99 from 0.4 to 1.5 µm, greater than 0.93 from 1.5 to 2.0 µm, and 0.66 to 0.93 at wavelengths longer than 2.0 µm (Polyanskiy 2018).

- An optical-grade mirror can specularly reflect nearly 90% of incident sunlight (curve C in Figure 6).

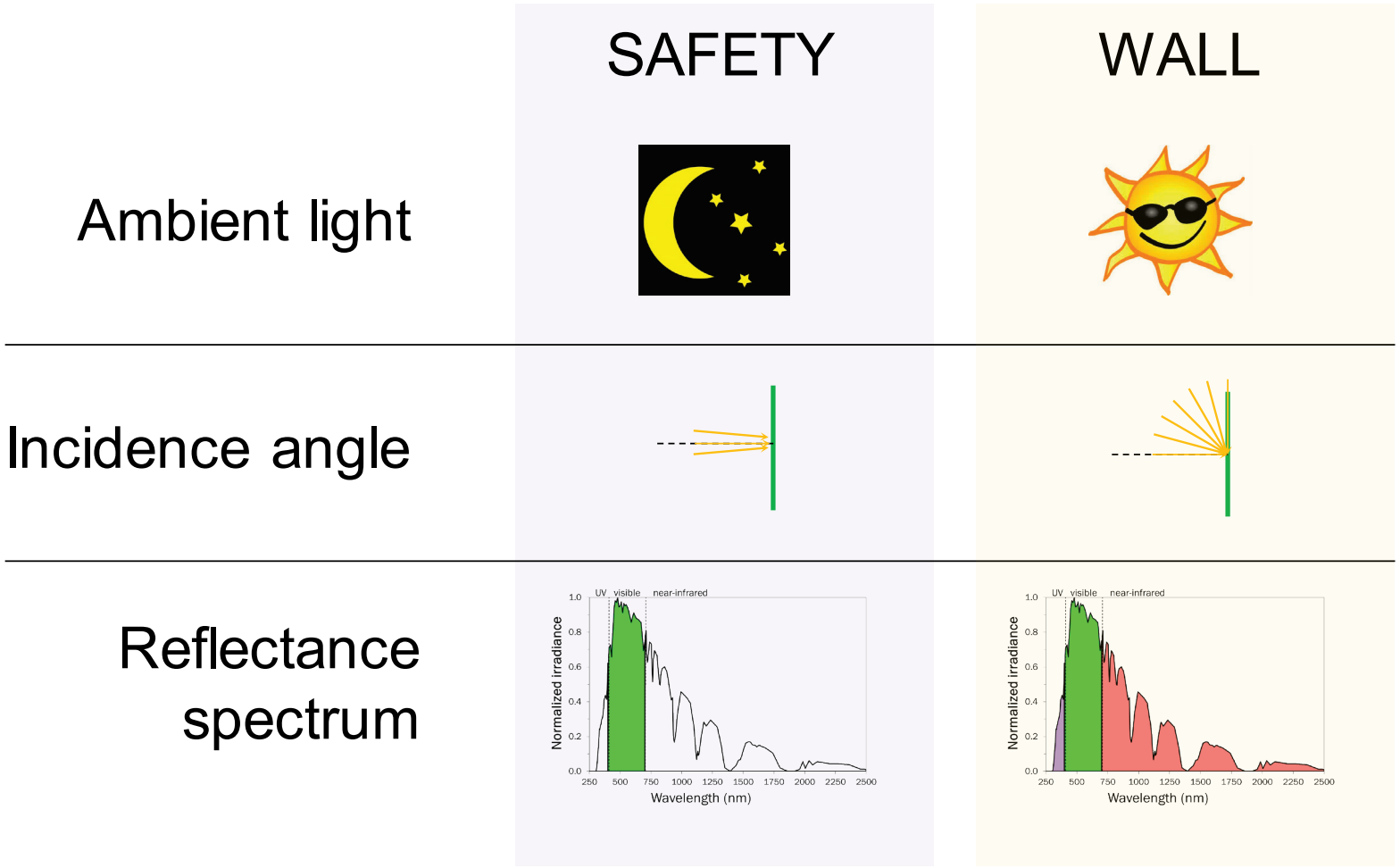

Figure 5. Compared to safety retroreflectors, wall retroreflectors must reflect a larger fraction of incident sunlight, over a wide range of incidence angles and wavelengths.

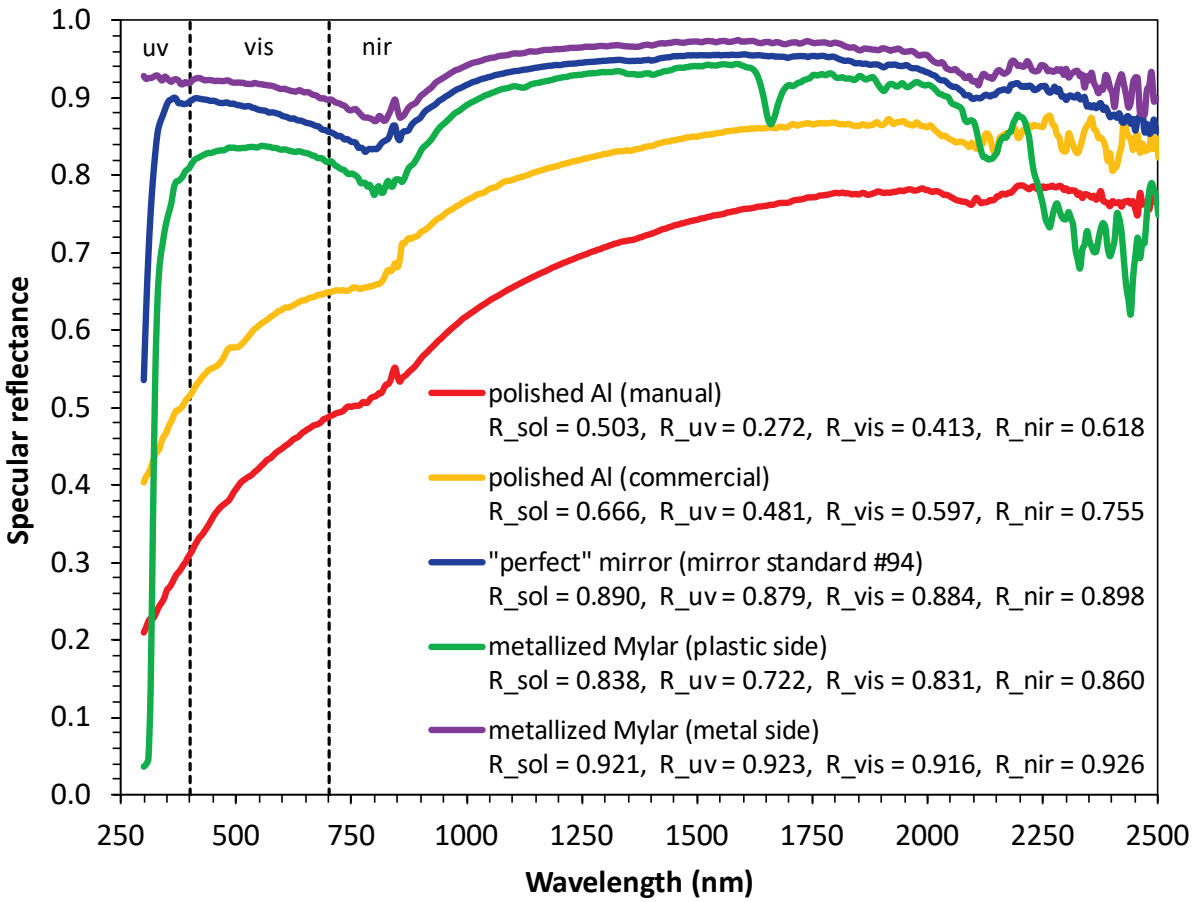

Figure 6. Specular components of solar spectral reflectances of five mirrorlike systems, including a manually polished block of aluminum (curve B); a mirror calibration standard (curve C); a commercially polished aluminum sheet (curve D); the metal face of aluminized Mylar (curve E); and the plastic face of aluminized Mylar (curve F).

2.2 Angular distribution of solar irradiation

To explore the distribution of angles at which beam sunlight strikes walls, we computed hourly solar positions and hourly beam irradiances on isolated walls following the procedure detailed in the Task 2.3 report: *Using solar availability to scale HVAC savings.* That is, we calculated beam tilt irradiance with the standard isotropic sky model (Duffie and Beckman 2006), using as inputs (a) global horizontal and diffuse horizontal hourly solar irradiation values from Typical Meteorological Year 3 (TMY3) weather files (NREL 2018b) and (b) mid-hour solar positions computed with the Measurement and Information Data Center Solar Position and Intensity (MIDC SOLPOS) Calculator provided by the National Renewable Energy Laboratory (NREL 2018a). Ground albedo was set to 0.20. We then calculated in each season (e.g., summer = June/July/August) the variation with solar altitude of the cumulative fraction of wall-incident solar energy.

To illustrate, consider summer sunlight in Fresno, CA. About 85%, 37%, 35%, and 1% of the beam radiation incident on a north, east, west, or south wall arrives when the solar altitude angle is less than or equal to 30˚ (Figure 7). Since the incidence angle of beam radiation striking a wall will always equal or exceed the solar altitude angle, less than 37% of the beam radiation striking the east or west wall, and essentially none of that striking the south wall, will do so at an incidence angle less than or equal to 30˚.

Table 1 summarizes by U.S. climates (Figure 8) and wall direction the distribution with solar altitude angle of beam sunlight incident in summer.

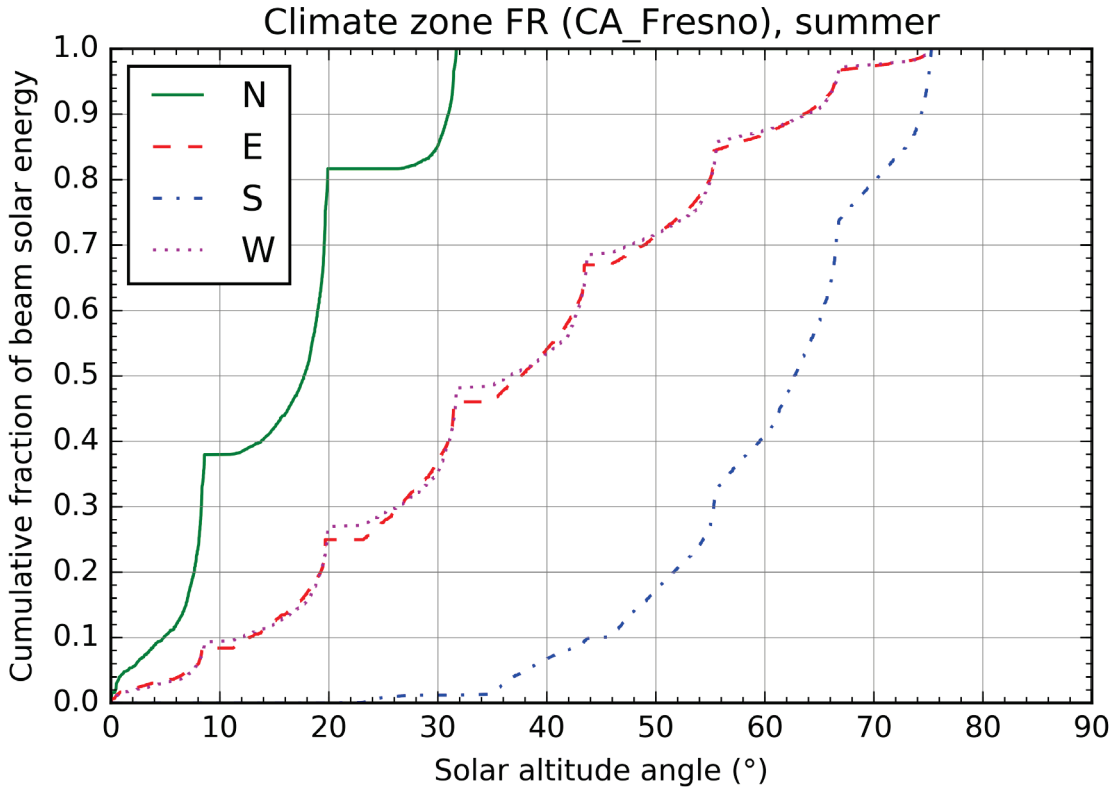

Figure 7. Variation with solar altitude angle of the cumulative fraction of beam solar energy incident on an isolated north (N), east (E), south (S), or west (W) wall in Fresno, CA during the summer months (June/July/August).

Table 1. Percentage of beam sunlight incident on an isolated north, east, south, or west wall in summer at solar altitude angles up to 5, 15, 30, 45, 60, or 75°, reported for the climates shown in Figure 8.

	(a) north						(b) east						(c) south						(d) west					
Climate	**5°**	**15°**	**30°**	**45°**	**60°**	**75°**	**5°**	**15°**	**30°**	**45°**	**60°**	**75°**	**5°**	**15°**	**30°**	**45°**	**60°**	**75°**	**5°**	**15°**	**30°**	**45°**	**60°**	**75°**
1A	0	22	62	88	99	100	0	9	30	54	78	95	0	0	1	6	27	73	1	4	22	49	73	97
2A	5	37	78	98	100	100	2	10	32	56	82	97	0	0	1	7	30	80	0	9	31	53	79	99
2B	30	60	90	100	100	100	6	18	37	62	84	100	0	0	0	10	32	90	6	15	36	60	82	100
3A	9	34	81	100	100	100	2	9	33	63	85	98	0	0	1	9	40	86	2	9	31	65	86	98
3B	3	28	82	99	100	100	1	8	40	62	83	97	0	0	1	7	30	80	1	9	28	61	85	98
BU	8	26	84	100	100	100	2	9	34	65	85	98	0	0	1	8	36	85	2	5	33	62	84	97
FR	10	42	85	100	100	100	3	12	37	67	87	99	0	0	1	10	41	95	3	12	35	69	87	99
3C	23	51	94	100	100	100	3	9	35	59	84	100	0	0	1	10	42	97	5	13	33	63	89	100
4A	21	51	93	100	100	100	1	8	36	64	87	100	0	0	1	11	45	100	6	15	35	70	88	100
4B	17	45	92	100	100	100	6	15	45	65	86	98	0	0	1	7	35	86	3	12	31	61	85	98
4C	28	71	99	100	100	100	3	13	37	68	96	100	0	0	2	20	74	100	4	16	40	75	94	100
5A	11	48	92	100	100	100	2	11	36	70	90	100	0	0	1	15	52	100	1	9	36	67	88	100
5B	17	59	100	100	100	100	4	16	41	69	93	100	0	0	2	16	62	100	3	13	46	70	92	100
6A	35	68	97	100	100	100	5	15	39	73	92	100	0	0	2	19	64	100	7	17	41	73	92	100
6B	16	55	100	100	100	100	3	15	45	71	96	100	0	0	2	18	71	100	3	12	44	69	96	100
7	22	67	99	100	100	100	2	14	42	70	96	100	0	0	2	20	72	100	4	17	39	75	94	100
8	50	89	100	100	100	100	14	38	69	97	100	100	0	0	12	77	100	100	1	7	51	93	100	100

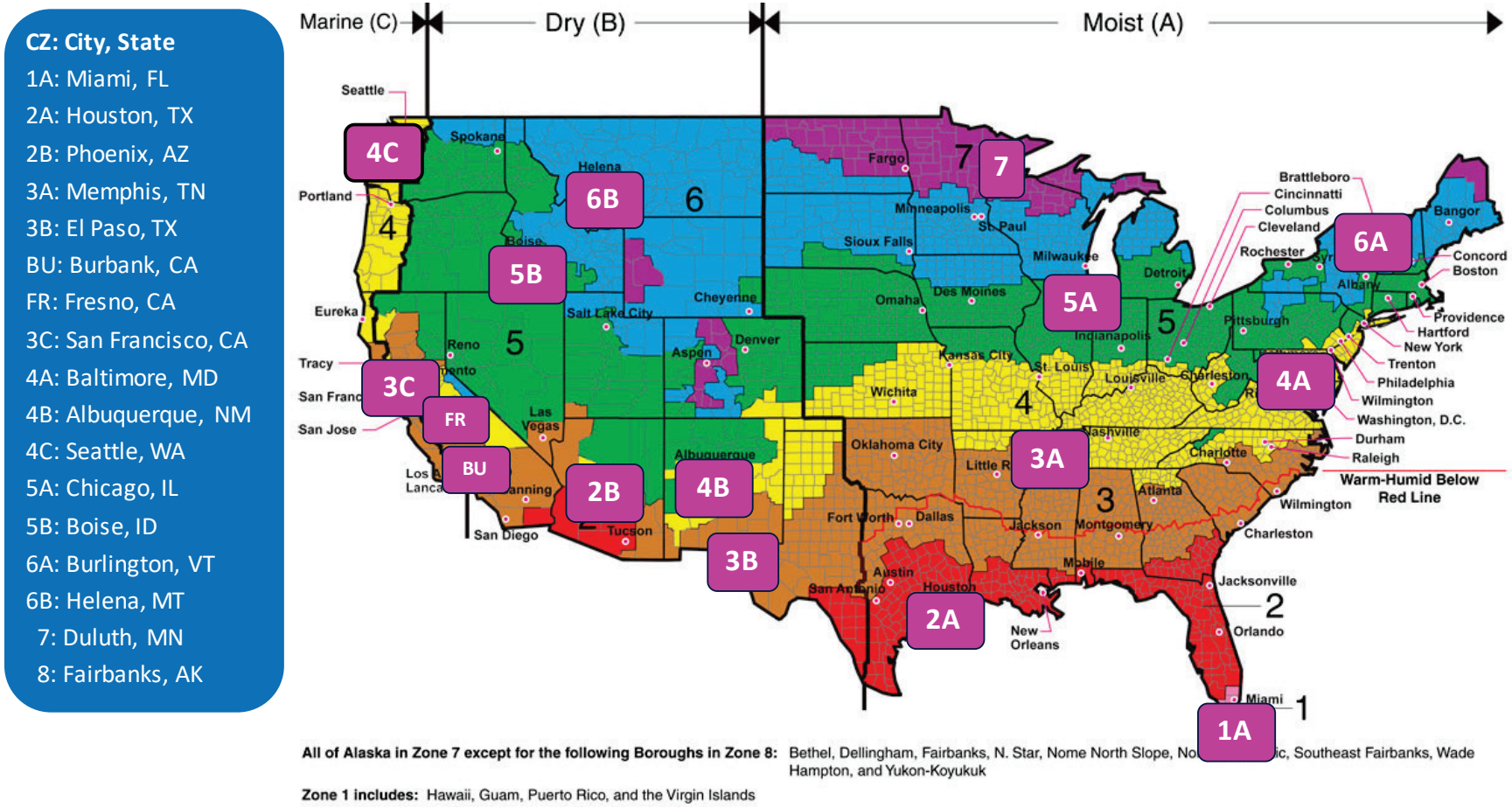

Figure 8. Map of U.S cities representing ASHRAE climate zones (CZ) 1 – 8, plus two California cities (Burbank and Fresno). Adapted from Briggs et al. (2003a,b).

2.3 Vertical surface retroreflection vs. solar altitude angle

The preceding analysis indicates that systems that retroreflect only near-normal light may not work well when applied to south, east, and west walls.

Consider beam sunlight incident on the vertical symmetric two-surface retroreflector shown in Figure 9. A beam of altitude angle $\alpha < 45°$ in the plane of page will strike face 1 at incidence angle $\theta_1 = \alpha + \gamma = \alpha + (90° - \beta) = 45° + \alpha$. The beam reflected from face 1 will strike face 2 at incidence angle $\theta_2 = 180° - 90° - \theta_1 = 45° - \alpha$. The beam reflected from face 2 will be anti-parallel to original solar beam, completing the retroreflection.

2.3.1 Case 1: Metal mirror faces

If each surface is metal mirror, the system will retroreflect beam sunlight incident on face 1 when $\alpha < 45°$; retroreflect beam sunlight originally incident on face 2 when $\alpha = 45°$; and reflect specularly upward, but not to its origin, beam sunlight originally incident on face 2 when $\alpha \neq 45°$. The latter flux will go directly to the sky when $\alpha < 45°$, or to the sky via face 1 when $\alpha > 45°$.

2.3.2 Case 2: Transparent faces

If each surface is made of the same transparent material with $n \geq 1.5$, face 1 will exhibit TIR for $\alpha < 45°$ because the beam incidence angle $\theta_1 = 45° + \alpha$ will always exceed the material's critical angle in air, θ_c (Figure 10). However, the beam reflected from face 1 will be reflected by face 2 only if $\theta_2 = 45° - \alpha$ exceeds θ_c. The maximum solar altitude α_{max} at which face 2 will total internally reflect the beam from face 1 beam ranges from 3.2° for low-index glass (n=1.5) to 20.4° for diamond (n=2.4) (Table 2). When $\alpha_{max} < \alpha < 45°$, beam light reflected from face 1 will pass through face 2. Meanwhile, beam sunlight originally incident on face 2 will strike at angle $\theta_2 = 45° - \alpha$. If $\theta_2 < \theta_c$, it will pass through face 2. Otherwise, it will be reflected specularly upward, in some cases striking face 1. Reflected light that strikes face 1 will be reflected to the sky since $\theta_1 = 45° + \alpha > \theta_c$. Thus, beam sunlight incident originally incident on either face 1 or face 2 will pass through face 2 when $\theta_2 = 45° - \alpha \leq \theta_c$, or $\alpha \geq 45° - \theta_c$.

Inspection of the 5° altitude columns in Table 1(b-d) indicates that if made of low-index glass or plastic ($n = 1.5$, $\theta_c = 3.2°$), this system will transmit, rather than retroreflect, nearly all beam sunlight incident on an east, south, or west wall in summer.

Table 2. Real refractive indices and critical angles of some transparent materials.

Material	Real refractive index	Critical angle in air (°)	Maximum solar altitude yielding total internal reflection at face 2 (°)
Low-index glass [a]	1.5	41.8	3.2
High-index glass [b]	2.0	30.0	15.0
Cubic zirconia	2.2	27.0	18.0
Diamond	2.4	24.6	20.4

[a] Such as Schott N-BK7 crown glass (Polyanskiy 2018).

[b] Such as Ohara Glass lanthanum S-LaH79 (Polyanskiy 2018).

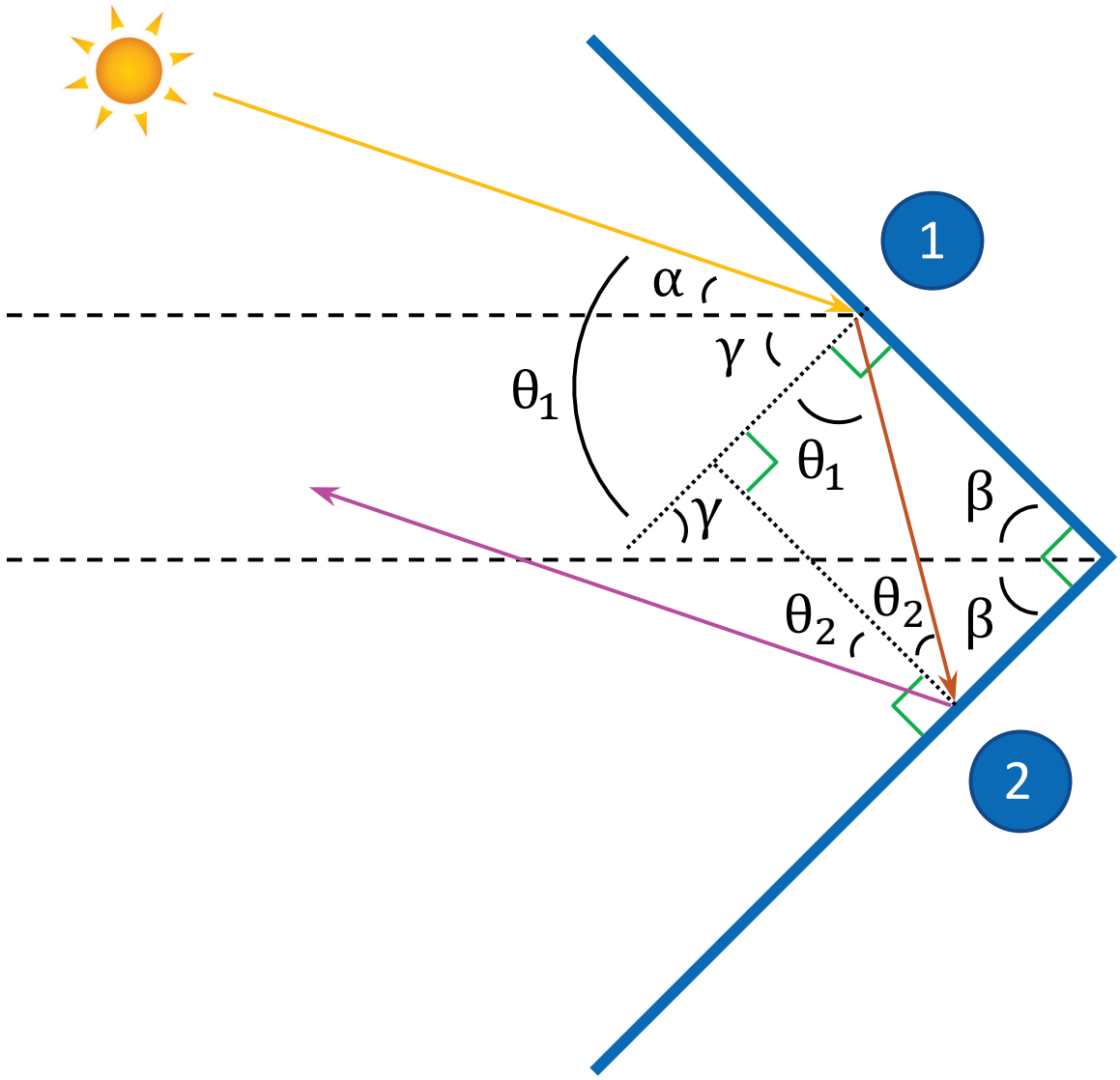

Figure 9. Angles of incidence and reflectance at faces of a vertical symmetric two-surface retroreflector (isosceles right triangle formed by orthogonal faces 1 and 2 and their undrawn vertical hypotenuse; β=45°).

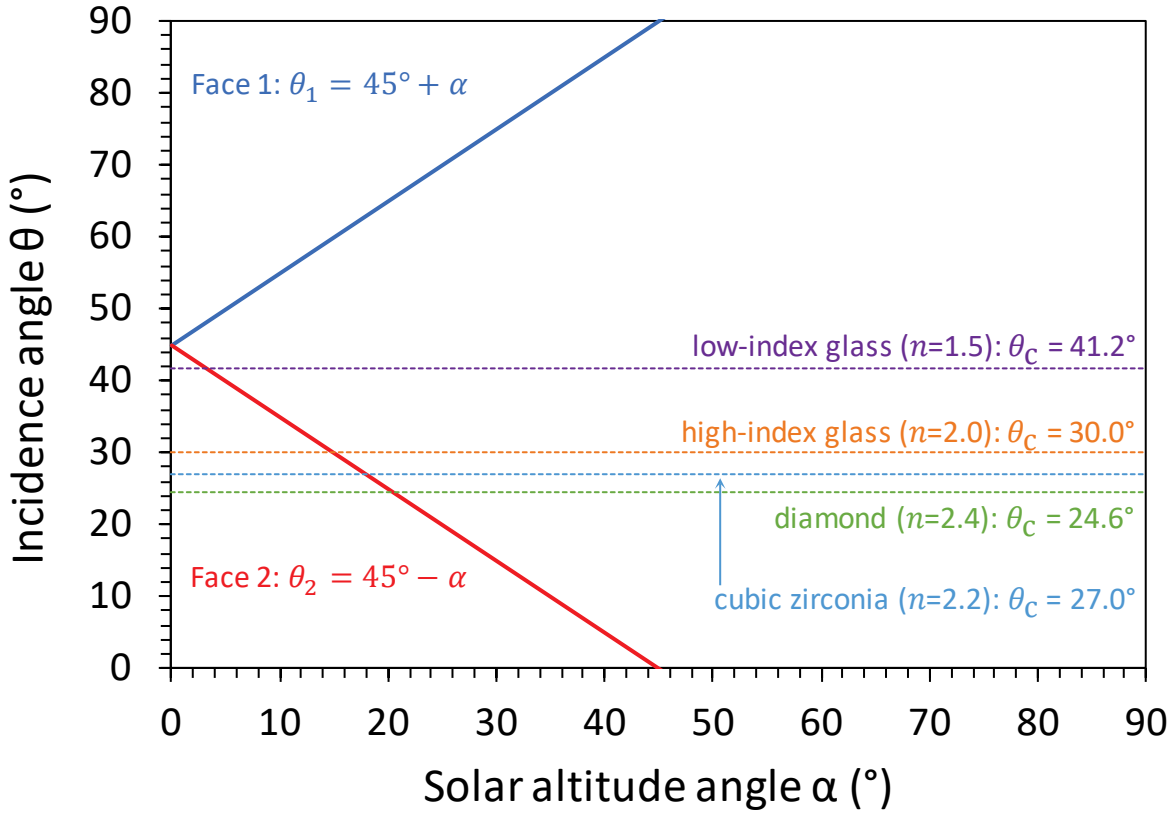

Figure 10. Angles of incidence on when downwelling beam sunlight strikes face 1, and beam-light reflected from face 1 strikes face 2, in the vertical retroreflector system drawn in Figure 9. Shown for reference are the critical angles for various clear windows in air.

3 Ray-tracing simulations

We used the open-source Ray Optics Simulation web application (Tu 2018) to simulate a variety of 2-D vertical retroreflectors.

3.1 Designs

Each "symmetric" design comprises an array of pairs of equal length faces forming an isosceles right triangle with a vertical hypotenuse and 45° acute angles. Each "asymmetric" design comprises an array of pairs of unequal length faces (upper face length 5, lower face length 3.3) forming a right triangle with a vertical hypotenuse and acute angles of 33.5° (top) and 56.5° (bottom). Low and high-index glasses follow the specifications of Table 2.

a) Symmetric empty mirrors, where light passes from air to ideal metal mirrors.

b) Symmetric empty mirrors behind a low-index glass vertical window, to keep the mirrors clean.

c) Asymmetric empty mirrors.

d) Asymmetric empty mirrors behind a low-index glass vertical window.

e) Symmetric low-index glass right triangular prisms.

f) Symmetric low-index glass right triangular prisms with ideal metal mirror backing replacing the glass-air interface.

g) Asymmetric low-index glass right triangular prisms.

h) Asymmetric low-index glass right triangular prisms with ideal metal mirror backing.

i) Symmetric high-index glass right triangular prisms.

j) Symmetric high-index glass right triangular prisms with ideal metal mirror backing.

k) Asymmetric high-index glass right triangular prisms.

l) Asymmetric high-index glass right triangular prisms with ideal metal mirror backing.

3.2 Results

Figure 11 shows the paths of beams incident from altitudes of α = 0, 15, 30, 45, 60, and 75°. The following observations are limited to the six altitudes simulated.

3.2.1 Prisms

- As predicted in Section 2.3.2, design *e* retroreflects only at $\alpha = 0^\circ$ and design *i* retroreflects only at $\alpha = 0$, 15, and 30°. The retroreflection at $\alpha = 30^\circ$ by design *i* is simply specular reflection.
- Design *g* does not work.
- Design *k* fares poorly at $\alpha = 0^\circ$, provides mixed results at $\alpha = 30^\circ$, and works well at $\alpha > 30^\circ$.
- Mirror backings (designs *f*, *h*, *j*, and *l*) help a bit, but reflect some light downward.

3.2.2 Empty mirrors

- Design *a* provides a combination of retroreflection and not-to-origin upward reflection.
- Design *c* fares poorly at $\alpha = 0^\circ$, provides mixed results at $\alpha = 30^\circ$, and works well at $\alpha > 30^\circ$.
- Placing the mirrors behind a vertical window (designs *b* and *d*) has little effect.

From these analyses we conclude that design *a* (symmetric empty mirrors) is the logical starting point for prototype fabrication, and that it can kept clean behind a low-index window (design *b*) without performance penalty.

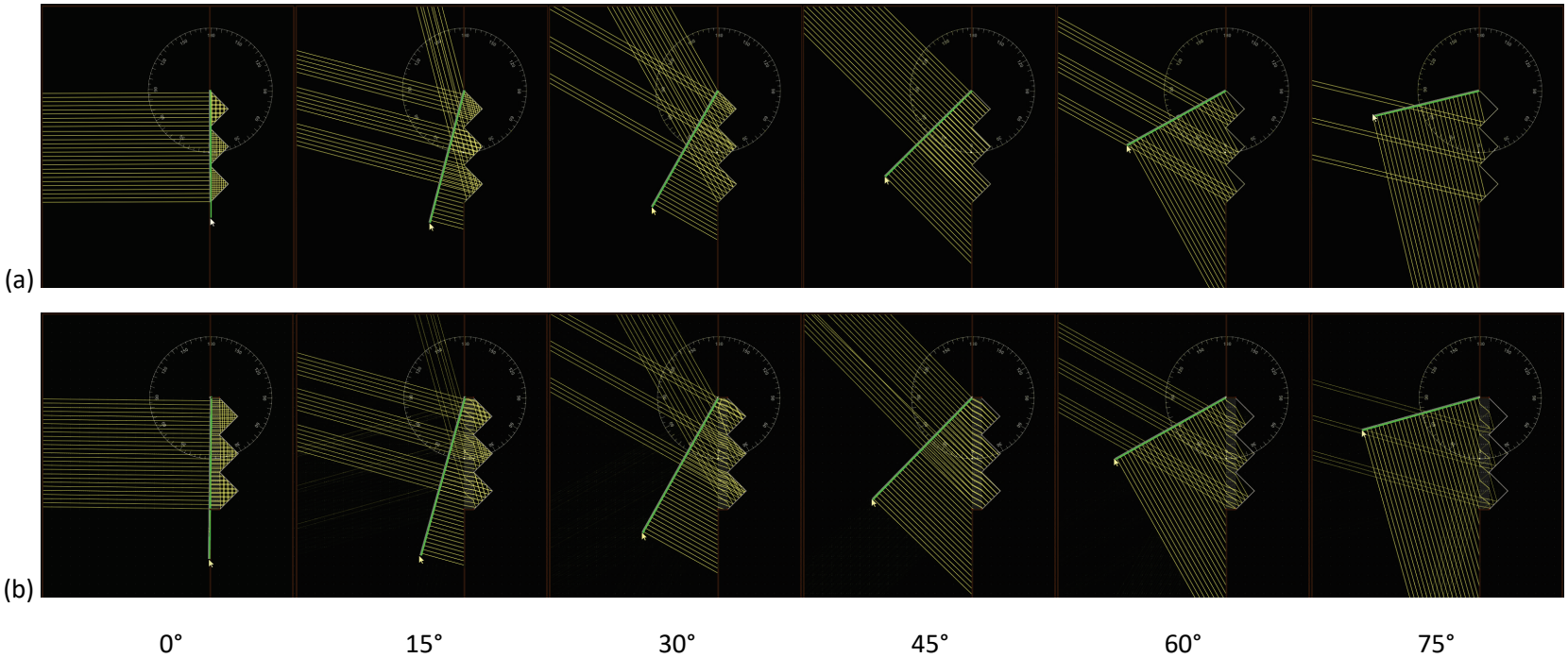

Figure 11. Reflection of beam light as a function of beam altitude angle, shown for a variety of two-surface retroreflectors. Shown here: (a) symmetric empty mirrors; (b) symmetric empty mirrors behind a low-index glass window (n=1.5).

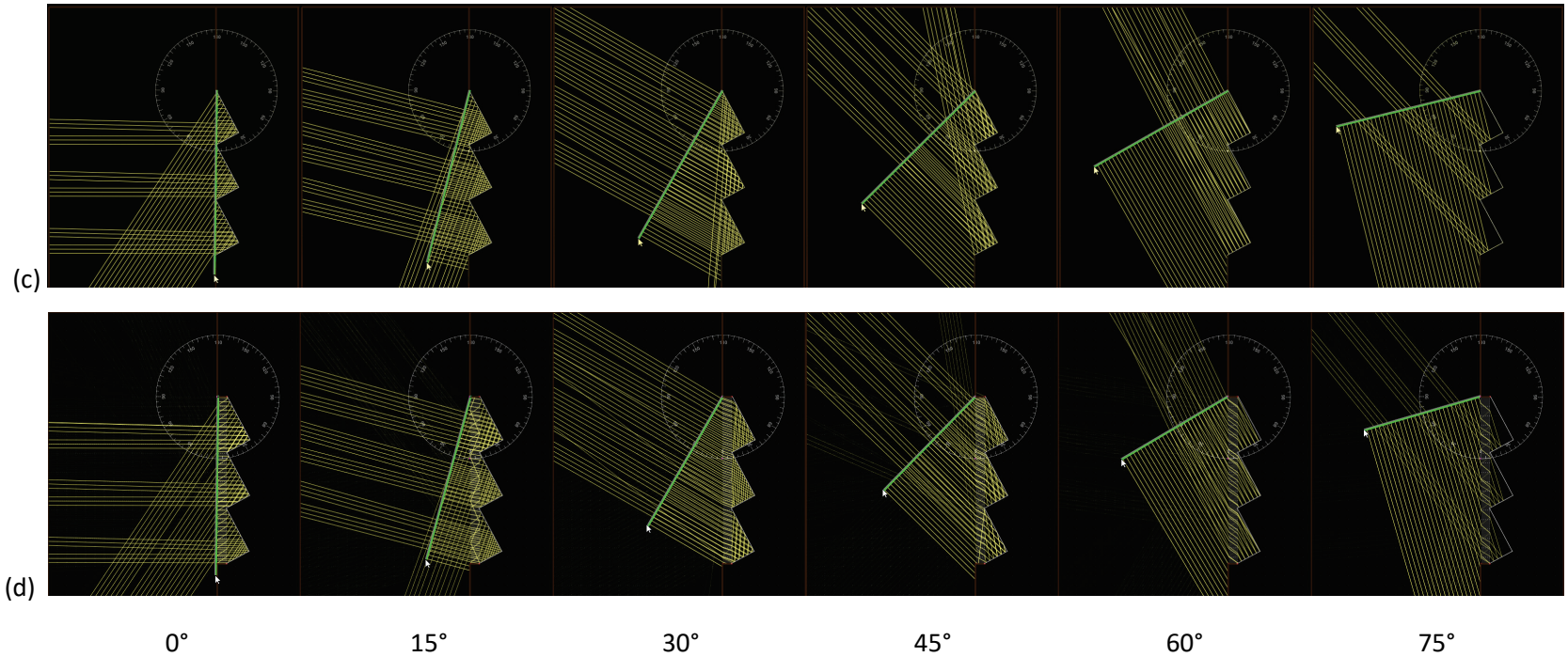

Figure 11 (continued). Shown here: (c) asymmetric empty mirrors; (d) asymmetric empty mirrors behind a low-index glass window (*n*=1.5).

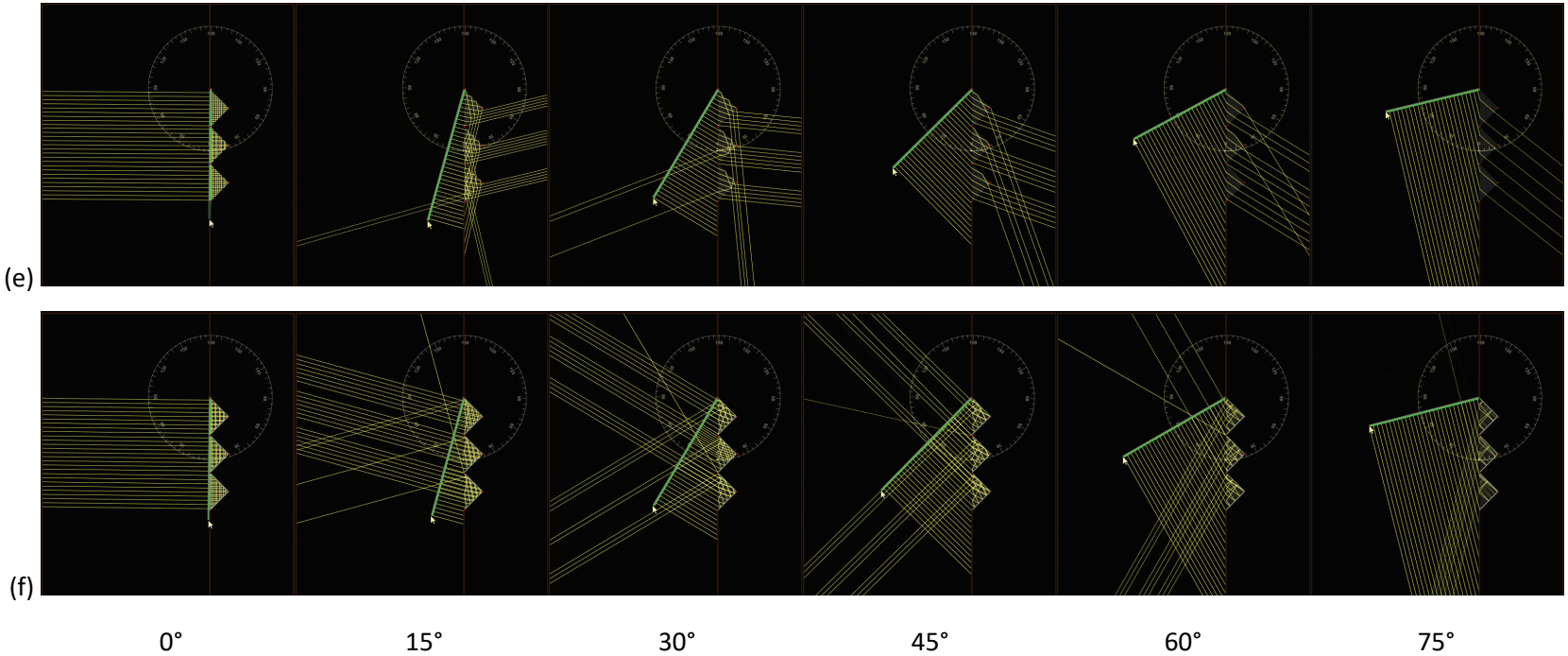

Figure 11 (continued). Shown here: (e) symmetric low-index glass (n=1.5) right triangular prisms; (f) system *e* plus mirror backing.

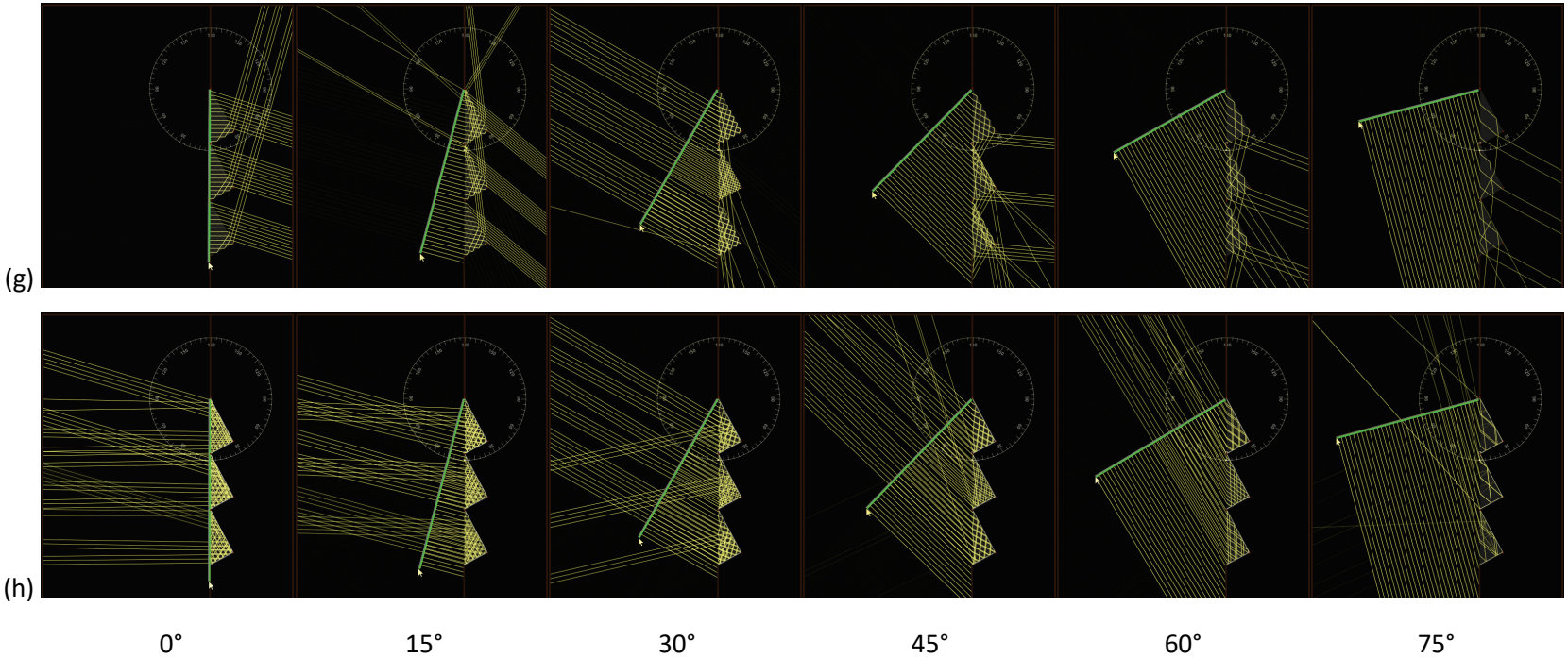

Figure 11 (continued). Shown here: (g) asymmetric low-index glass (n=1.5) right triangular prisms; (h) system *g* plus mirror backing.

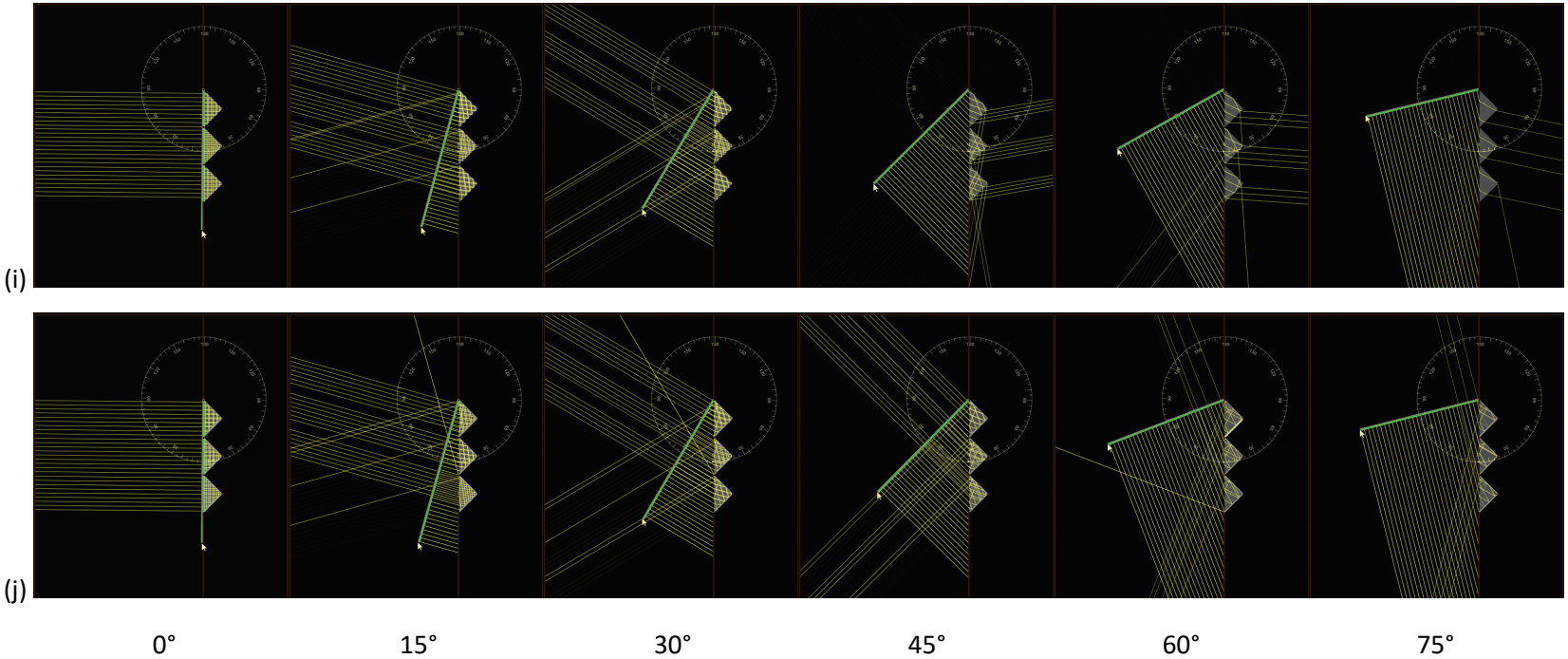

Figure 11 (continued). Shown here: (i) symmetric high-index glass (n=2.0) right triangular prisms; (j) system *i* plus mirror backing.

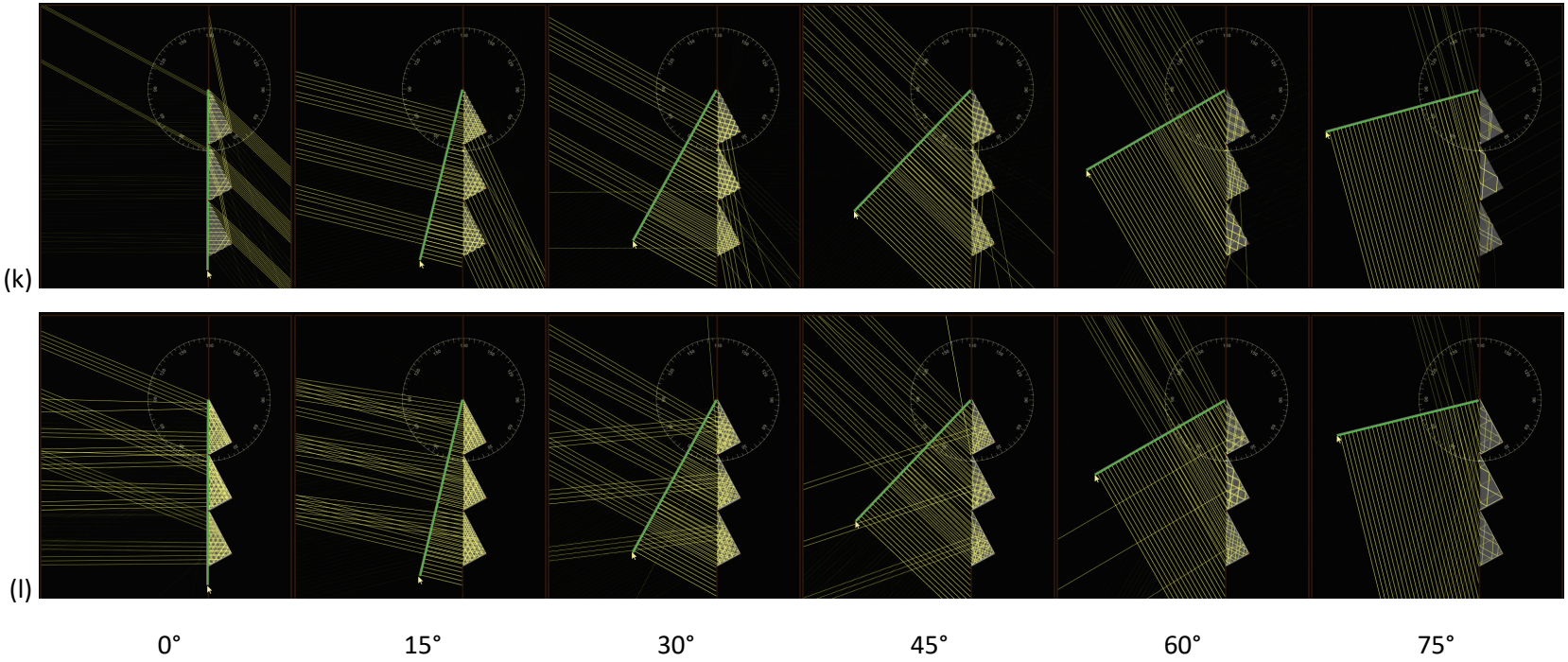

Figure 11 (continued). Shown here: (k) asymmetric high-index glass (*n*=2.0) right triangular prisms; (l) system *k* plus mirror backing.

4 Instrumentation

We assessed retroreflection with two instruments: a simple, monochromatic goniometer that we built in-house, and a sophisticated solar spectral gonionometer designed and operated by Dexerials, a project partner.

4.1 Simple goniometer

The simple goniometer comprises a vertical laser (violet[1], wavelength 405 nm) that shines upward through a small (~ 2 mm) central hole in a hole in a cardboard box. The box is lined with a printed sheet of paper bearing a series of concentric rings that mark the angle (5˚ to 75˚ in 5˚ increments) at which light is reflected from a specimen mounted on a turnable spit. A camera looking down on the box can records images of the light patterns formed within the rings (Figure 12).

The angle of Fresnel (first-surface) reflection equals the angle of incidence on the specimen. The intensity of the retroreflection (if any) can be compared to that of Fresnel reflection (Table 3).

Table 3. Fresnel reflectances of p (parallel)-polarized light (R_p), s (perpendicular)-polarized light (R_s), and unpolarized light ($\bar{R}$) in air striking a surface of real refractive index 1.5 at incidence angle θ, computed following Georgia State University (2005).

θ (°)	5	10	15	20	25	30	35	40	45	50	55	60	65	70	75
R_p	0.04	0.04	0.04	0.03	0.03	0.03	0.02	0.01	0.01	0.00	0.00	0.00	0.01	0.04	0.11
R_s	0.04	0.04	0.04	0.05	0.05	0.06	0.07	0.08	0.09	0.11	0.14	0.18	0.23	0.30	0.40
$\bar{R}$	0.04	0.04	0.04	0.04	0.04	0.04	0.04	0.05	0.05	0.06	0.07	0.09	0.12	0.17	0.25

Patterns of light reflection from the three specimens shown in Figure 13—a mirror calibration standard, a polished aluminum panel with brush marks, and a white retroreflective safety film—can be seen in Figure 14.

As expected, each specimen yields a specular (Fresnel) reflection, but only the safety film exhibits retroreflection. The intensity of this retroreflection can be compared to that of the Fresnel reflection at 70˚, which ranges from 0.04 to 0.30 if the laser beam is polarized, or is 0.17 if the laser beam is unpolarized (Table 3).

We recommend rotating a linearly polarized laser beam to orient its electric field perpendicular to the plane of incidence (that containing the surface normal and incident ray). This will raise

[1] There was no special reason to use a violet laser; we simply had one available.

its Fresnel reflectance to its maximum (s-polarized) value R_s, making it easier to compare retroreflection to Fresnel reflection. The upper and lower images in Figure 14c show maximum and minimum specular reflectances observed when rotating the incident laser beam. The rotations corresponding to these two images were approximately 90° apart.

4.2 Advanced goniometer

Dexerials' advanced spectro-goniometer (Figure 15) measures solar spectral bi-directional reflectance from 0.350 to 2.350 µm. Its design and operation are detailed by Harima and Nagahama (2017).

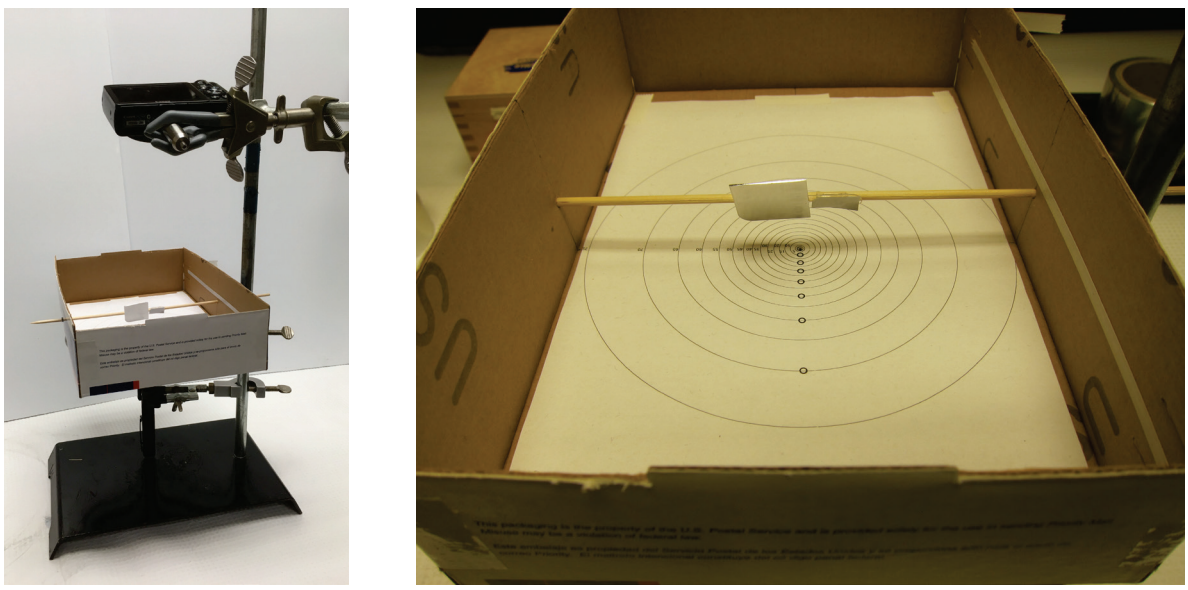

(a) (b)

Figure 12. We built a simple goniometer to compare retroreflection to specular reflection (~ 5%). (a) side view of goniometer with laser pointer shining up and camera looking down; (b) top view of goniometer, showing specimens (aluminum panel at left; white retroreflective safety film at right) mounted on rotatable spit, central hole admitting laser beam, and concentric rings (5° to 75° in 5° increments) marking angle of reflection.

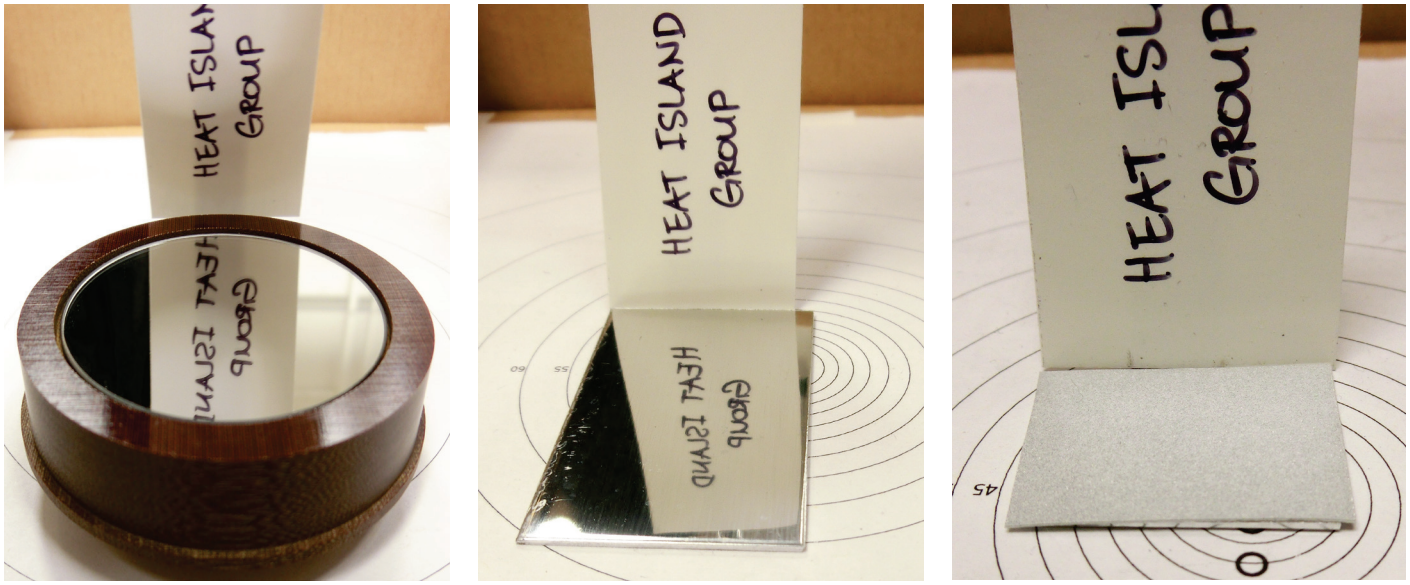

(a) (b) (c)

Figure 13. Three surfaces tested in the simple goniometer: (a) mirror calibration standard; (b) polished aluminum panel with brush marks; and (c) white retroreflective safety film.

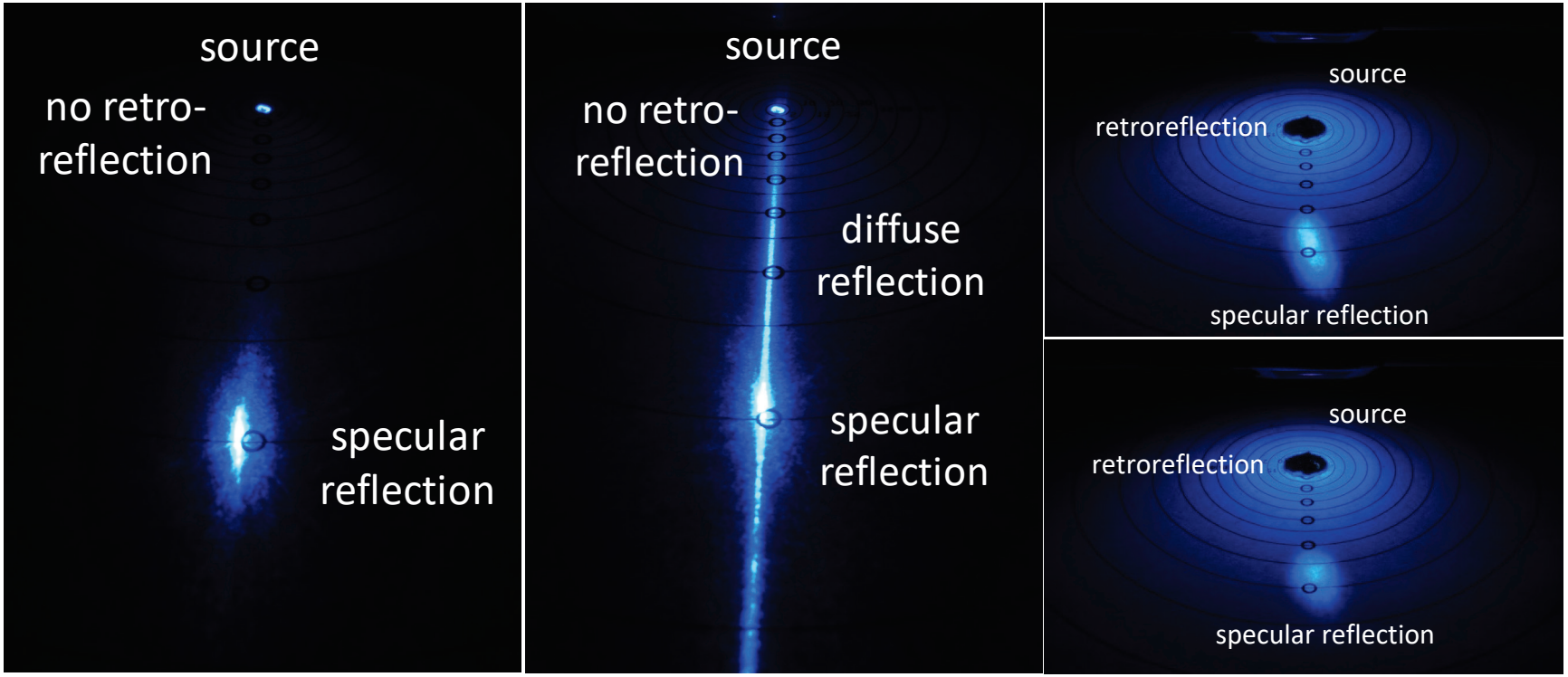

(a) (b) (c)

Figure 14. Simple goniometer images of laser light at 70° incidence reflected from (a) mirror calibration standard, exhibiting purely specular reflection; (b) polished aluminum panel, exhibiting specular and diffuse reflections; and (c) a white retroreflective safety film, exhibiting specular reflection and retroreflection. Upper and lower images in panel (c) show maximum and minimum specular reflectances observed when rotating incident laser beam.

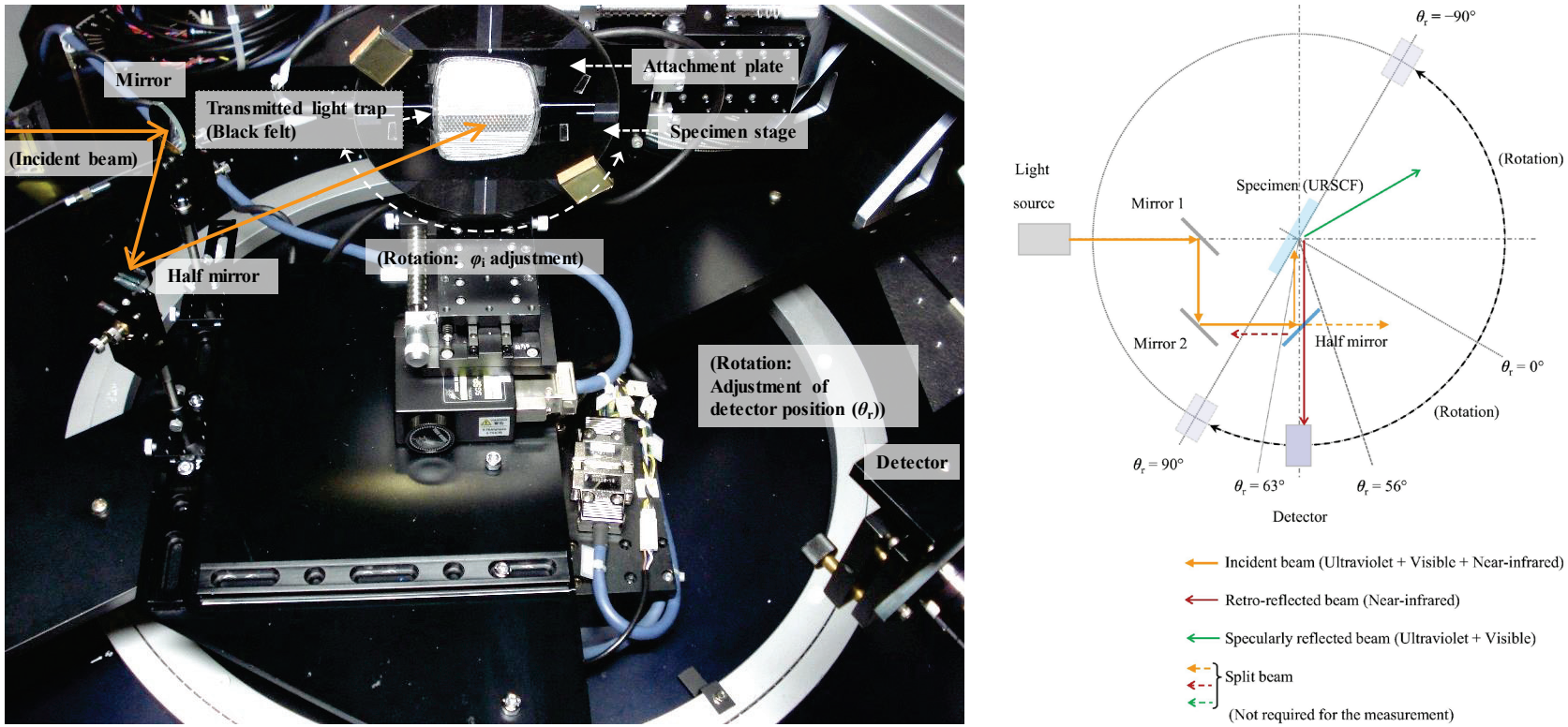

(a) (b)

Figure 15. Dexerials' advanced spectro-goniometer measures solar spectral bi-directional reflectance. Source: Harima and Nagahama (2017)

5 Prototype development and evaluation

5.1 Safety films

Examination in the simple goniometer of retroreflections and Fresnel reflections from several safety films (e.g., the white film in Figure 13c and Figure 14c) showed that the retroreflection was often weaker than the Fresnel reflectance, which we in turn estimated to be about 0.04 to 0.17 (Table 3).

5.2 Bicycle retroreflector

We tested the retroreflectance of several specimens of a clear prismatic bicycle reflectors in three conditions:

a) bare (Figure 16, left and middle segments in each photo);

b) with a third of the rear coated with LO/MIT low-E radiative barrier paint (Figure 16, right segment in each photo); and

c) with about 0.4 μm of aluminum sputtered on the rear (Figure 17).

Specimen *b* was abandoned after inspection with the simple goniometer indicated that the LO/MIT coating did not enhance retroreflection. We measured the near normal-hemispherical solar spectral reflectances of the two remaining two specimens (*a* and *c*) with a Perkin-Elmer Lambda 900 UV-vis-NIR spectrometer equipped with 150 mm Labsphere integrating sphere (Figure 18). We then sent them to Dexerials for characterization in the advanced goniometer.

Figure 19 shows the visible and near-infrared (NIR) bi-directional reflectance intensities of the bare reflector (panel a) and the aluminum coated reflector (panel b). Retroreflection from each specimen is evident at incidence angles of 15 and 30°, with a small hint of retroreflection at 45° from the coated specimen. In each case the magnitudes of the visible and NIR retroreflectors are similar, and diminish as incidence angle increases. The aluminum coating increased Fresnel reflection and reduced retroreflection. Since retroreflection essentially vanishes at incidence angles exceeding 30°, these specimens do not seem promising for wall application.

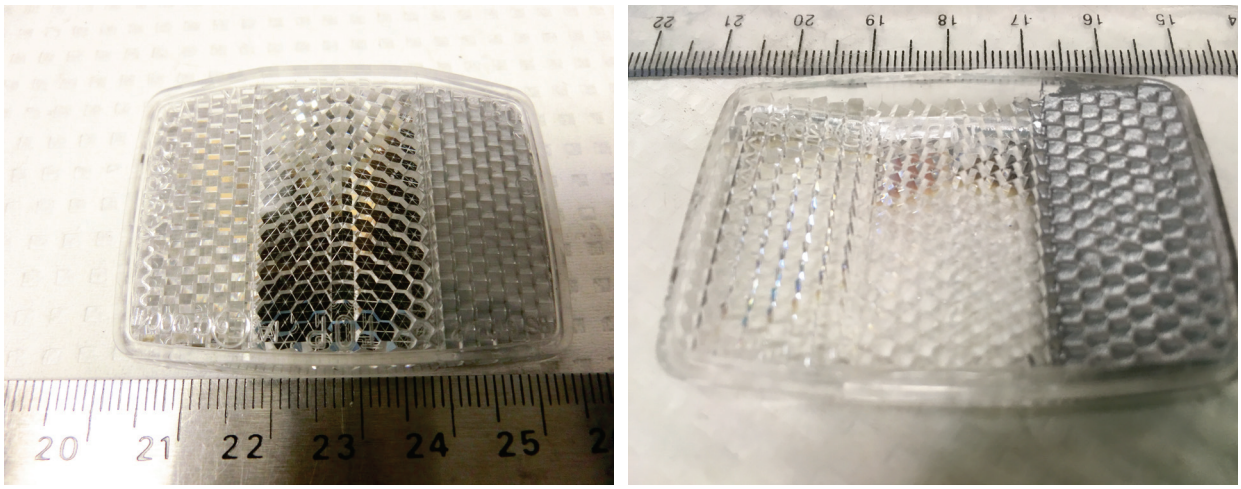

(a) front **(b) back**

Figure 16. Front and rear faces of a clear plastic bicycle retroreflector showing right third of back surface coated with LO/MIT low-E radiative barrier paint. Rulers are marked in centimeters.

(a) front **(b) back**

Figure 17. Front and rear faces of another clear plastic bicycle reflector with about 0.4 μm of aluminum sputtered on its rear.

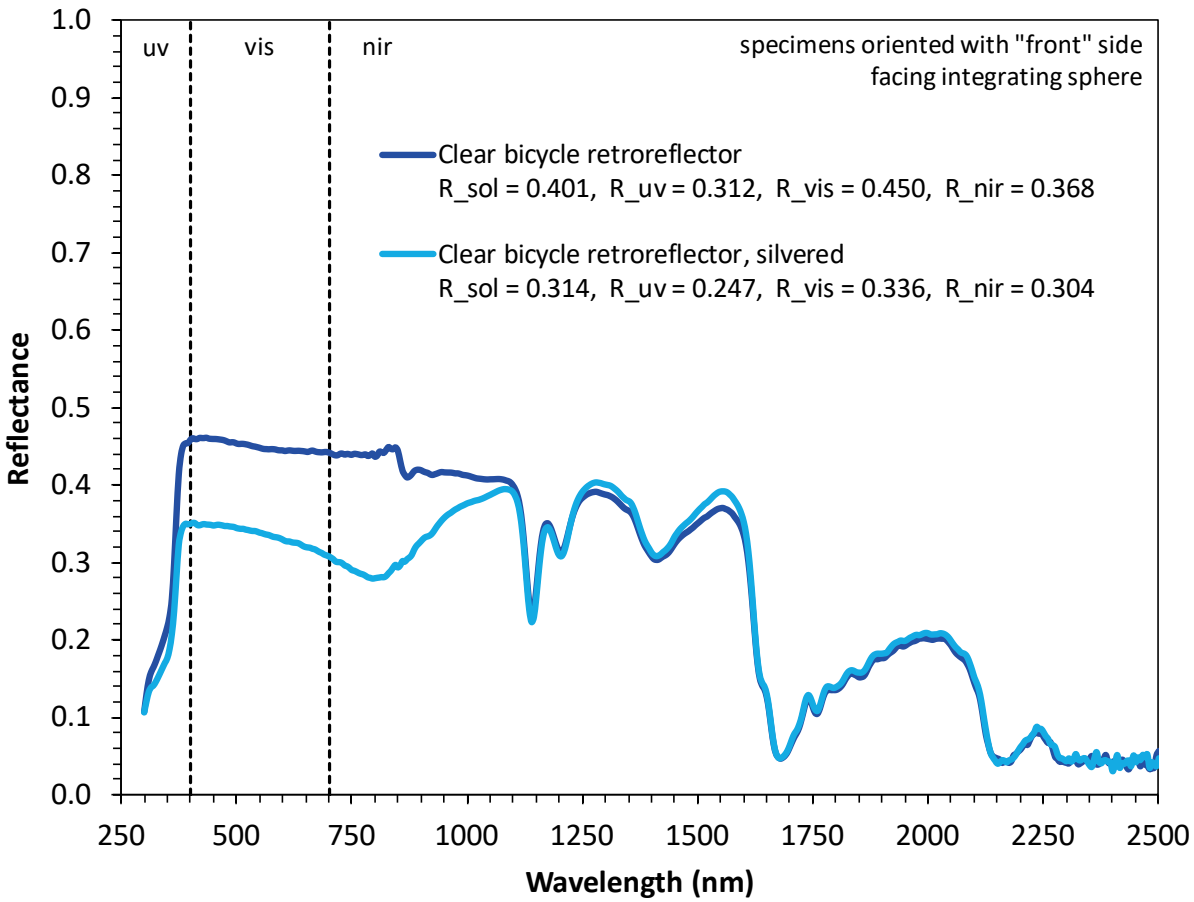

Figure 18. Near normal-hemispherical solar spectral reflectance of front of bicycle retroreflector before and after sputtering aluminum on its back surface.

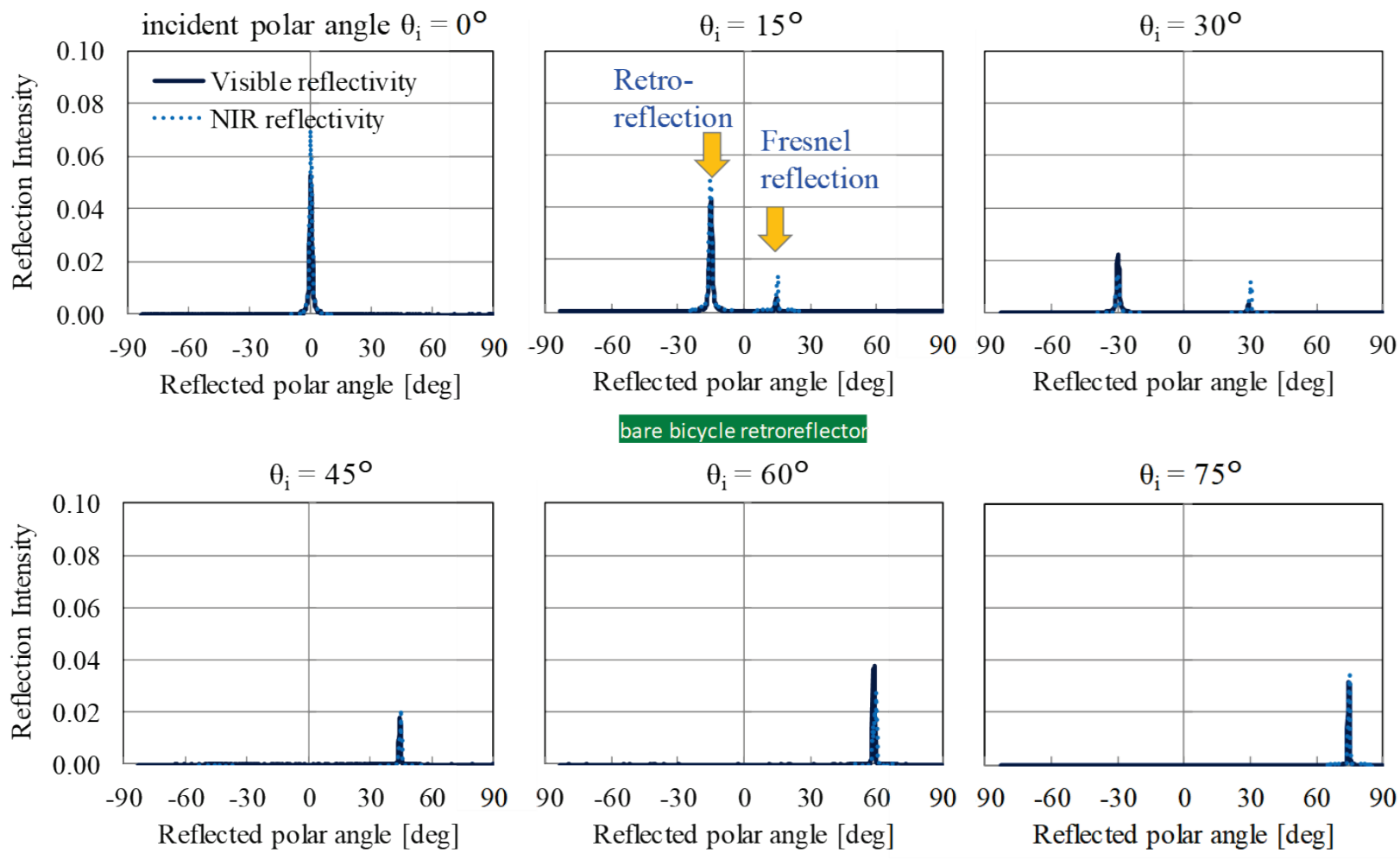

(a)

Figure 19. Bi-directional reflectance intensities of (a) bare bicycle retroreflector and (b) aluminum-coated bicycle retroreflector, courtesy Dexerials.

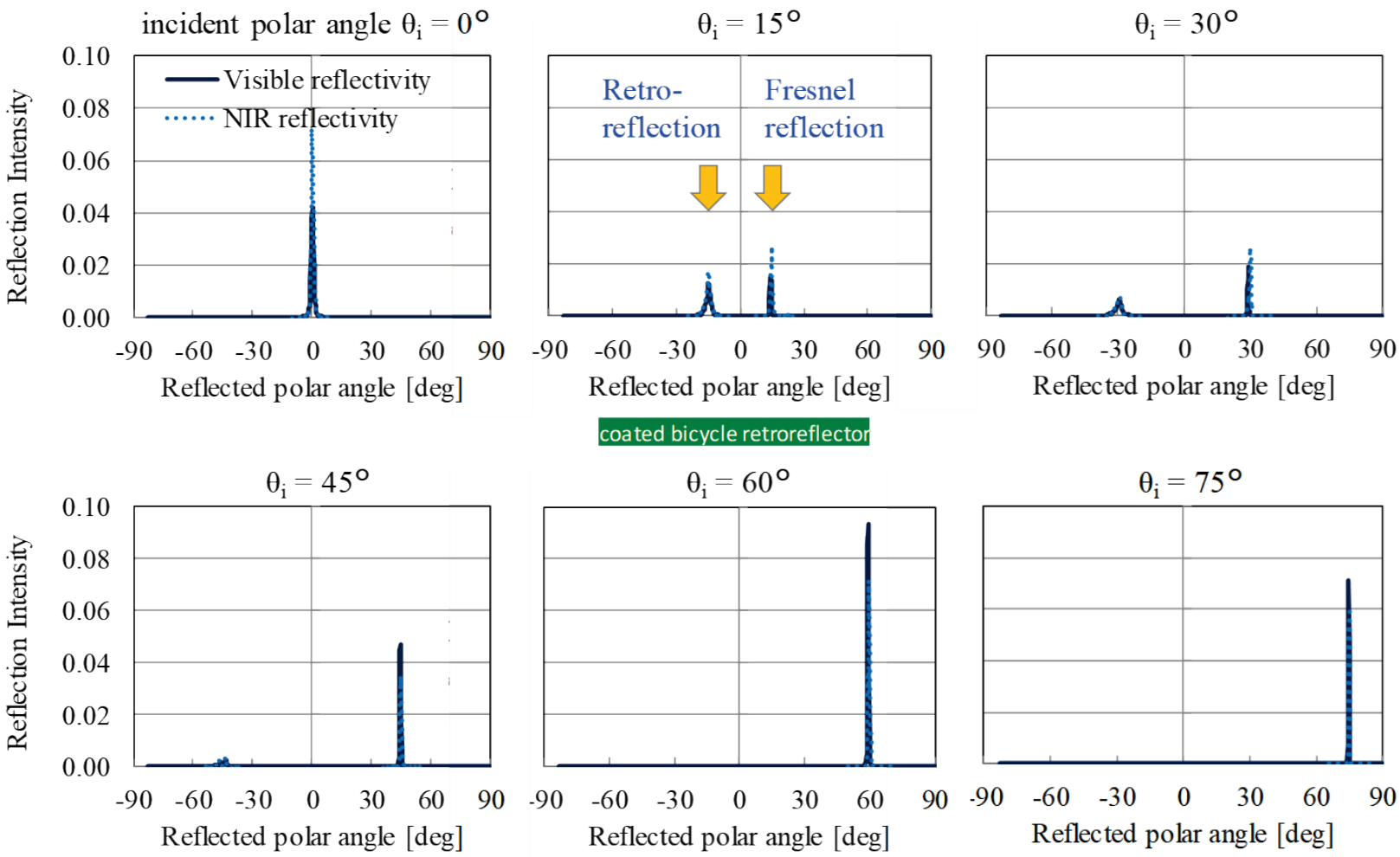

(b)

Figure 19 (continued).

5.3 ABS plastic groove retroflector

We hired a 3-D printing service to fabricate ABS plastic pieces with orthogonal grooves, onto which we planned to sputter a thin coating aluminum following the same process used to coat the bicycle reflector. However, stairsteps found in the groove faces—an issue that we tried, but failed, to avoid by printing the pieces standing tall—suggested that a thin aluminum coating would also be jagged, and unlikely to provide the specular reflections needed for retroreflection.

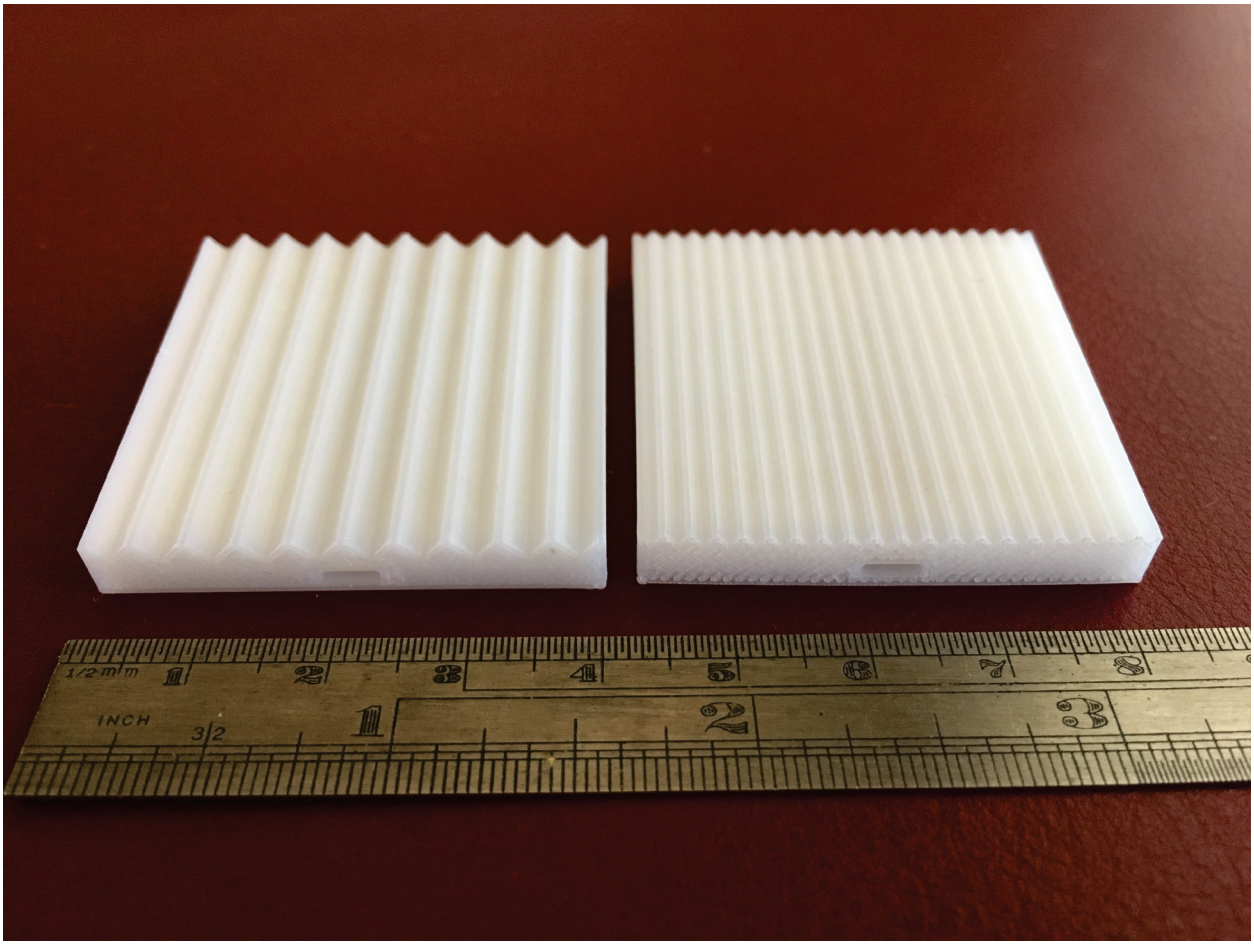

Figure 20. Right-angles grooves 3D printed in ABS plastic. Left: 4-mm pitch; right: 2-mm pitch.

5.4 Grooved aluminum block

We used a computer numeric control (CNC) milling machine to cut 2 mm pitch orthogonal grooves in an aluminum block (Figure 21). The grooves exhibited no retroreflection, so we manually polished them with a buffing wheel and paste (Figure 22). We also polished the rear of the block with the same tool and paste (Figure 22c, right image) to compare its specular spectral reflectance to that of a mirror standard (curves B and C in Figure 6).

We imaged the front and rear of the aluminum block, and the mirror standard, in the simple goniometer (Figure 23). It was hard to see retroreflection of the 405 nm violet laser beam from the polished grooves, possibly because at this wavelength the specular near-normal hemispherical reflectance of the polished block (as gauged by that of its rear) is about 0.31, making its two-bounce reflectance only $0.31^2 = 0.096$.

The simple goniometer allows for a comparative assessment of retroreflection by examining the brightness of light reflected towards the pinhole source. For flat surfaces, this assessment is more relevant at high incidence angles. The results from the mirror calibration standard (top row of Figure 23) provide an example of what we would see with a purely specular and non-retroreflective surface. The results from the hand-polished flat aluminum surface provide an example of what we would see with a non-retroreflective surface that reflects both specularly and diffusely. With these two samples as comparison, we interpret the hand-polished retroreflector prototype's more pronounced light intensities around the pinhole source at incidence angles greater than 50° to be evidence of some retroreflection (bottom row of Figure 23). Ultimately, however, the prototype reflects light at a wide range of angles over a wide range of incidence angles, so its performance in its current state is rather poor.

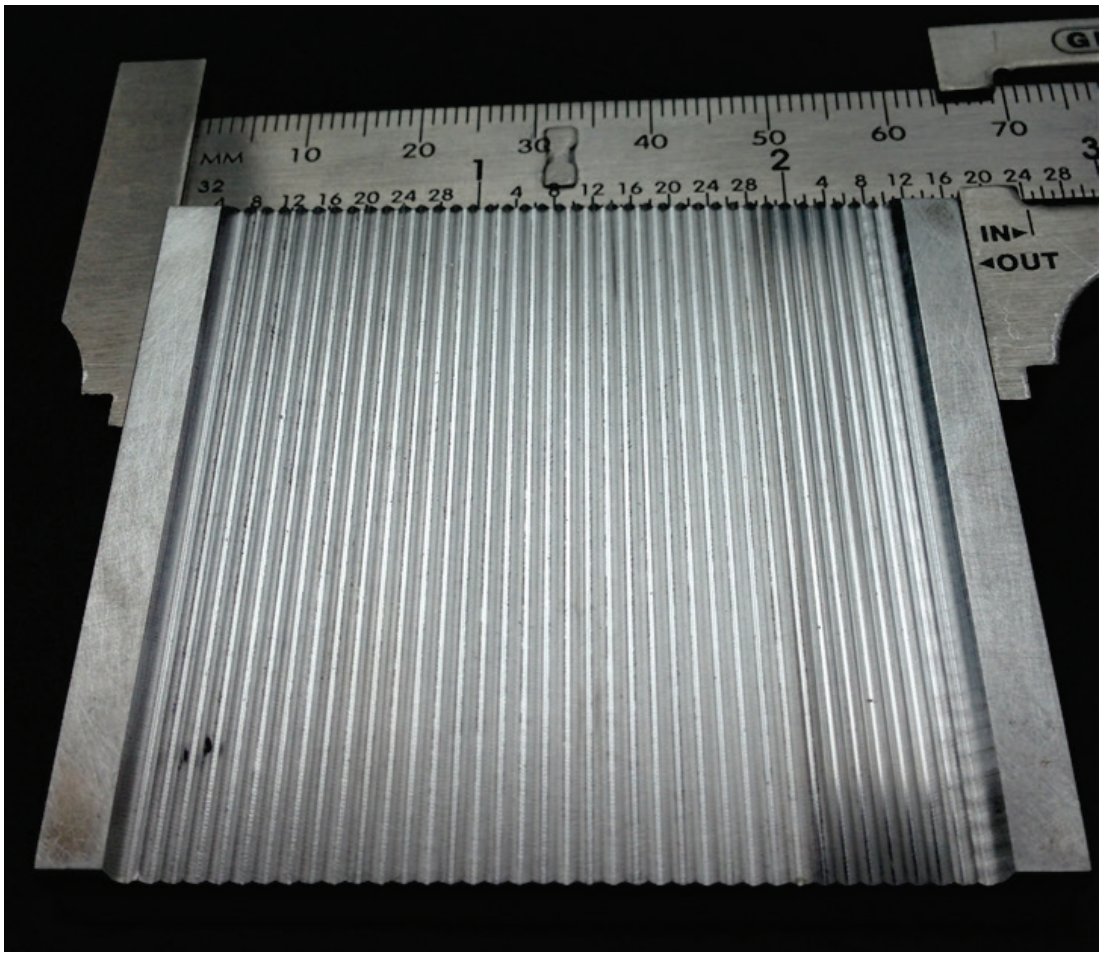

Figure 21. Unpolished aluminum block with 2-mm pitch right-angle grooves.

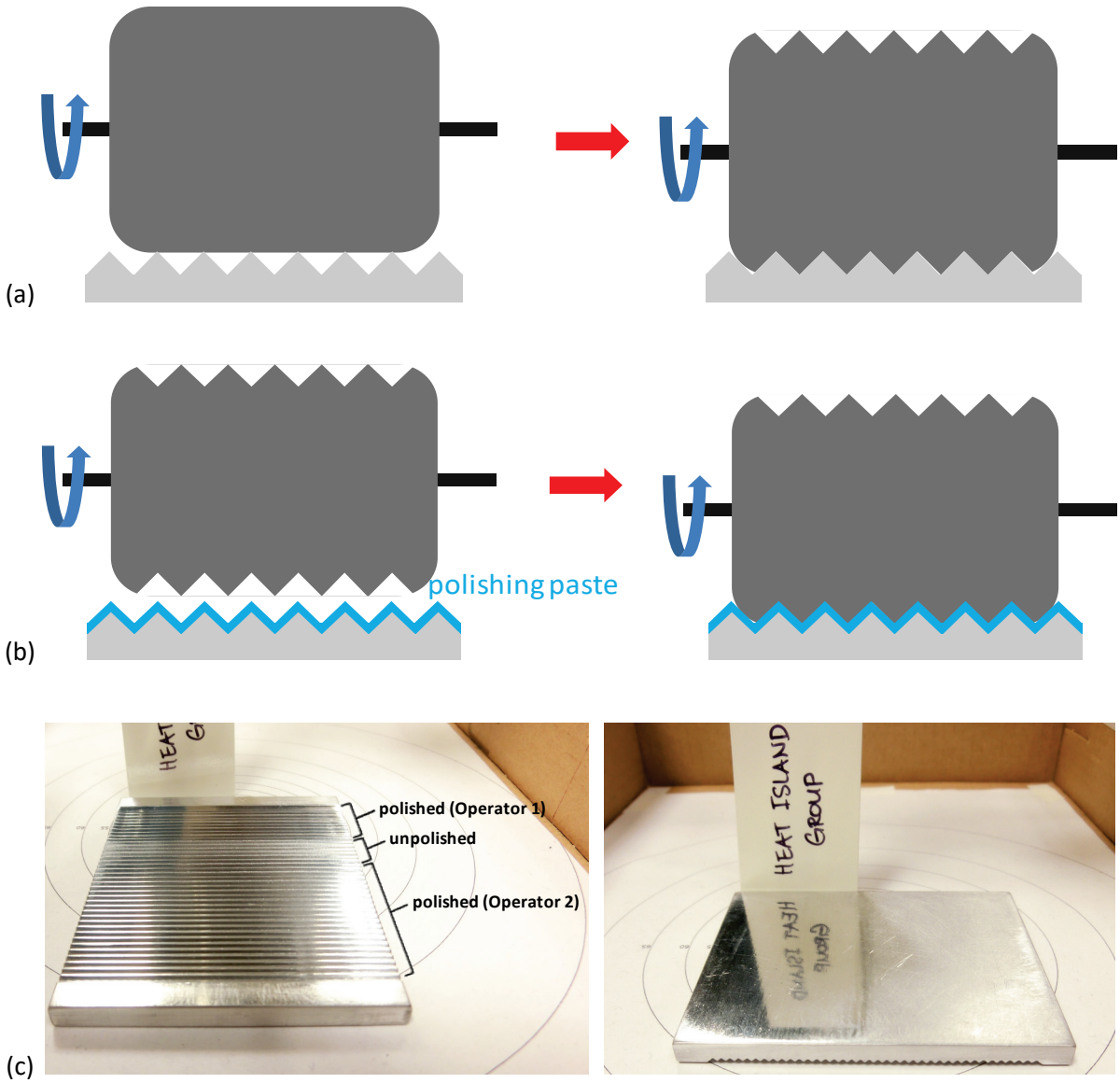

Figure 22. Polishing of right-angle groove aluminum block, showing (a) shaping of the buffing wheel; (b) polishing with paste; and (c) sections of the groove face polished by two different operators (left) and the back face smoothed by one of the operators (right).

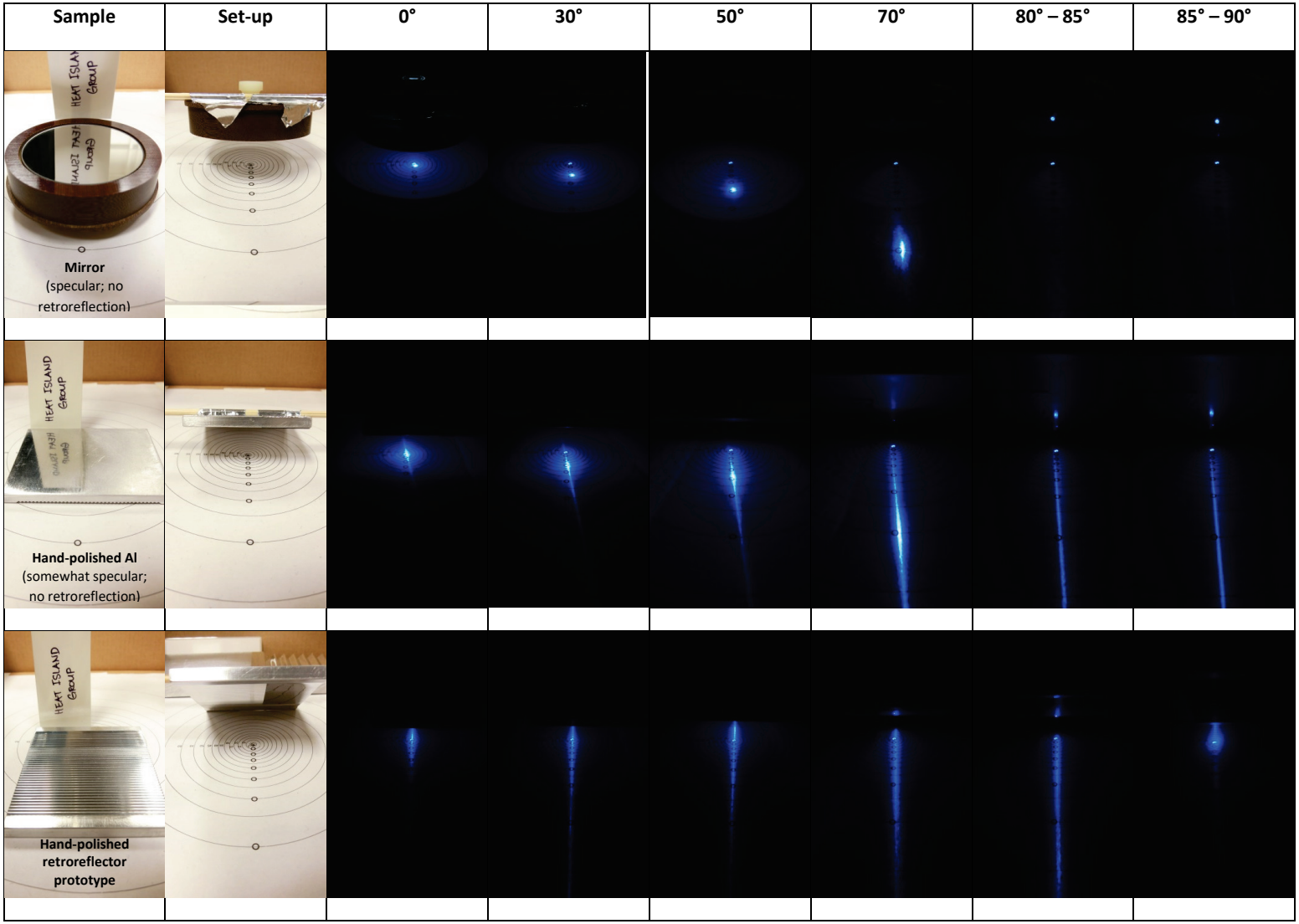

Figure 23. Reflections from three metal surfaces—a mirror reflectance standard, top row; the hand-polished rear face of the aluminum block, middle row; and the hand-polished grooved face of the aluminum block—imaged at incidence angles of 0 to nearly 90° in the simple goniometer.

5.5 Aluminized Mylar film

Aluminized Mylar film has very high specular reflectance across the solar spectrum, with a metal-face specular solar reflectance of about 0.92, and a plastic-face specular solar reflectance of about 0.84 (curves E and F in Figure 6). With the metal face forward, the two-bounce albedo could be $0.92^2 = 0.83$; with the plastic face forward, it could be $0.83^2 = 0.69$. The primary challenges appear to be forming orthogonal folds in the film and keeping the film flat. We are experimenting with creasing the film, stamping the film in a die, and even gluing or taping it to a smooth grooved surface (Figure 24).

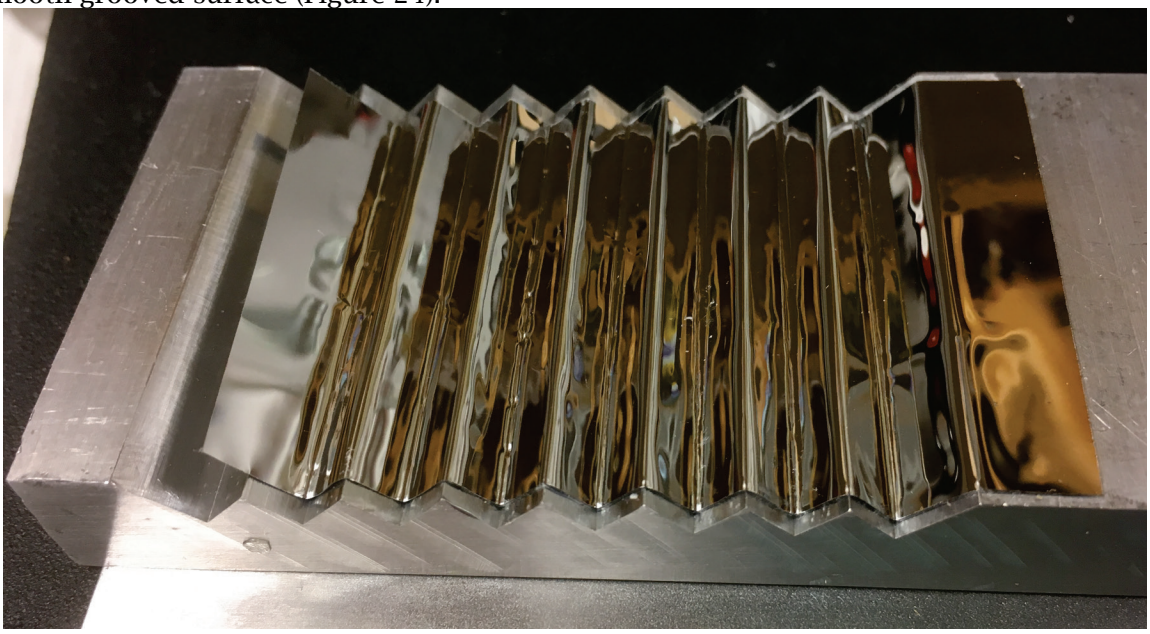

Figure 24. Aluminized Mylar adhered with double-sided tape to aluminum block with 7-mm pitch orthogonal grooves.

6 Summary

Raising a city's albedo increases the fraction of incident sunlight returned to outer space, cooling cities and their buildings. Retroreflective cool walls could improve upon diffusely reflecting cool walls by reflecting incoming beam radiation to the solar disc (if the retroreflection is three dimensional and ideal) or at least upwards (if the retroreflection is two dimensional and/or imperfect). For example, a retroreflective wall with albedo 0.60 could reflect 55% of incident sunlight to the sky, while a Lambertian wall of the same albedo would reflect only 36% of this light skyward.

The greatest challenge in retroreflective wall design appears to be the need to operate at large incidence angles to reflect a substantial portion of incident sunlight. First-principle physics and ray tracing simulations suggest that it will be difficult to achieve this with surfaces that rely on total internal reflection; this appears to be confirmed by solar spectral bi-directional reflectance

intensity measurements made on a prismatic bicycle reflector, and by comparison in a simple goniometer of the intensities of the Fresnel and retro reflections from prismatic retroreflective safety films.

Attempts to produce a two-surface retroreflector with orthogonal mirror grooves by cutting and polishing an aluminum block indicate that residual surface roughness impedes retroreflection. Ongoing efforts focus on shaping aluminized film Mylar, a material with very high specular reflectance across the solar spectrum.

Acknowledgements

We thank Dexerials for measuring the solar spectral bidirectional reflectance intensities of prototype retroreflectors.

References

ASTM. 2017. ASTM D4956-17: Standard Specification for Retroreflective Sheeting for Traffic Control. ASTM International. https://doi.org/10.1520/D4956-17

Duffie JA, Beckman WA. 2006. *Solar Engineering of Thermal Processes*, 3rd ed. Wiley.

Georgia State University. 2005. Hyperphysics tutorial: Fresnel's equations. http://hyperphysics.phy-astr.gsu.edu/hbase/phyopt/freseq.html#c1

Harima T, Nagahama T. 2017. Evaluation methods for retroreflectors and quantitative analysis of near-infrared upward reflective solar control window film — Part I: Theory and evaluation methods. *Solar Energy* 148, 177-192.

Levinson R, Akbari H, Berdahl P. 2010. Measuring solar reflectance—Part I: defining a metric that accurately predicts solar heat gain. *Solar Energy* 84, 1717-1744.

NREL. 2018a. Measurement and Information Data Center Solar Position and Intensity (MIDC SOLPOS) Calculator. National Renewable Energy Laboratory. https://midcdmz.nrel.gov/solpos/solpos.html .

NREL. 2018b. National Solar Radiation Data Base, 1991- 2005 Update: Typical Meteorological Year 3. National Renewable Energy Laboratory. http://rredc.nrel.gov/solar/old_data/nsrdb/1991-2005/tmy3

Polyanskiy MN. 2018. Refractive index database. http://refractiveindex.info

Tu R. 2018. Ray Optics Simulation web application. http://ricktu288.github.io/ray-optics